III 1.0

2.8 2.5

3.2 2.2

3.6

4.0 2.0

III 1.1

1.8

III 1.25 III 1.4 III 1.6

MICROCOPY RESOLUTION TEST CHART

DARDS-1963-A

AD-A164 309

86 2 14 004

DEPARTMENT OF THE AIR FORCE
AIR UNIVERSITY

# AIR FORCE INSTITUTE OF TECHNOLOGY

Wright-Patterson Air Force Base, Ohio

DTIC
ELECTE
S
FEB 14 1986
D

DTIC
S ELECTE
FEB 1 4 1986
D
D

A LASER FEEDBACK CONTROL DESIGN FOR
PASSIVE RING LASER GYROS IN A
VERY HIGH FINESSE CAVITY

THESIS

Mark A. Lorenz
Captain, USAF

AFIT/GE/ENG/85D-24

AFIT/GE/ENG/85D-24

A LASER FEEDBACK CONTROL DESIGN FOR PASSIVE RING

LASER GYROS IN A VERY HIGH FINESSE CAVITY

THESIS

Presented to the Faculty of the School of Engineering

of the Air Force Institute of Technology

Air University

In Partial Fulfillment of the

Requirements for the Degree of

Master of Science in Guidance and Control

Mark A. Lorenz, B.S.

Captain, USAF

December 1985

Approved for public release; distribution unlimited

## Preface

The purpose of this research was to lay the foundations for the development of a 58 $m^2$ passive ring laser gyro by constructing a smaller model which would address many of the problems associated with the larger gyro. For this passive gyro, a unique approach was tried, in which feedback controls were applied to a laser to match its frequency to the resonant frequency of the passive cavity.

I would like to thank my advisor, Lt Col Daniel J. Biezad, for directing my research in this area and for providing encouragement throughout the duration of the project. I would also like to thank my thesis sponsors, Maj James Rotge and Maj Gerald Shaw of the Frank J. Seiler Research Laboratory for providing the equipment and technical expertise for me to complete the work. I also appreciate the efforts of Mr. Bobby Hatfield of the Seiler Lab machine shop for his expert fabrication of all of the mounts and fasteners I had him construct for me. In addition, I would like to thank Dr. Jan Hall of the Joint Institute for Laboratory Astrophysics for his many ideas on how to attack this research. Thanks is also expressed to my committee members, Capt Steve J. Rogers, Dr. Won Roh, and Dr. Peter S. Maybeck for all their help critiquing this thesis and for their general technical advise. Lastly, I would like to thank my wife, Patricia, for all her patience and support during this effort.

— Mark Lorenz

# Table of Contents

## List of Figures

# List of Tables

AFIT/GE/ENG/85D-24

## Abstract

The Frank J. Seiler Research Laboratory is currently developing a Passive Resonant Ring Laser Gyroscope (PRRLG) enclosing 58 $m^2$ for proposed use in testing high precision rate sensors and for possibly validating the Theory of General Relativity. The sensitivities required for such experiments are in the $10^{-7}$ to $10^{-10}$ Earth Rate Unit (ERU) range. This high sensitivity necessitates the use of a large, high finesse cavity.

In dealing with high finesse cavities new considerations arise. For example, the cavity linewidth is narrower than linewidths of commercially available stabilized He-Ne lasers. The stability of the laser then becomes the limiting factor in the performance of the PRRLG because of the increased signal-to-noise ratio that arises in this situation. In addition, high finesse cavities exhibit photon lifetimes on the order of $10^{-3}$ to $10^{-6}$ seconds, which limits the bandwidth of practical controllers.

In this research, a PRRLG was constructed in which a He-Ne laser was frequency locked to a 25,000 finesse, 169 $cm^2$ resonant cavity, as opposed to the more traditional technique of locking the resonant condition of the cavity to the laser frequency. Using this configuration a random error of 0.0078 ERU for an averaging time of 10 seconds was

observed. The major error sources found in the gyro were identified and methods to eliminate them were proposed. Extrapolation of the performance of this PRRLG to the much larger 58 $m^2$ PRRLG, indicates the desired sensitivity for precision testing and relativity experiments is achievable.

# A LASER FEEDBACK CONTROL DESIGN FOR PASSIVE RING

# LASER GYROS IN A VERY HIGH FINESSE CAVITY

## I.   Introduction

### Background

The measurement of inertial rotation is of consider-
able interest in a number of areas, such as navigation, geo-
physics, and relativity (18:569).  For example, inertial
navigation systems used in aircraft and spacecraft criti-
cally depend on accurate inertial rotation sensors.  These
sensors provide measurements to the navigation system's
computer so that an accurate determination of the system's
orientation can be made.  The geophysical applications
include the measurement of the various effects that cause
fluctuations in the earth's rotation rate such as preces-
sion, nutation, wobble, and tidal-friction effects (3:172).
The accurate measurement of rotation is also important in
proposed experiments to validate the Theory of General
Relativity (7:88).

For the geophysical and relativity experiments,
the sensitivity required of the rotation sensor is on the
order of $10^{-7}$ to $10^{-10}$ Earth Rate Units (ERU) (18:569).
Research is being conducted at the Frank J. Seiler Labora-
tory to construct a rotation sensor approaching these per-
formance levels.  Current emphasis is on laser rate sensors,

as opposed to the traditional mechanical gyros, because the fundamental limits of performance are lower for the laser sensors. There are other important reasons to favor the laser sensor as described below.

Mechanical Gyroscopes. The most popular rotation sensor for many decades has been the mechanical gyroscope. Several forms of this type are in production, and they all rely on the high angular momentum of a spinning mass. Due to the high rotation rate, the gyros are subject to wear and, demonstrate Mean-Time-Between-Failures (MTBF) ranging from 1500 to 2000 hours.

Mechanical gyros typically require several minutes to spin-up and stabilize their internal temperature. This warm-up prevents degraded accuracy resulting from the numerous thermally related errors (19:26). These gyros have achieved drift rates of less than 0.001 degrees/hour, but are approaching a fundamental limit in precision (19:38), and thus have not been considered for the proposed high precision experiments.

Laser Gyroscope. With the development of a coherent, monochromatic light source, the laser, another type of rotation sensor made its debut when Rosenthal proposed two configurations of optical rotation sensors in 1961 (16:1143). These configurations which base their rotation measurements on the Sagnac Effect (17:708), were the

2

forerunners of active and passive Ring Laser Gyros (RLG) (Figure 1.1).

Rosenthal's proposed active RLG was implemented in 1962 by two Sperry engineers, Macek and Davis (11). As shown in Figure 1.2, this configuration used four Helium-Neon (He-Ne) plasma tubes and four external corner mirrors. Portions of the clockwise and counter-clockwise beams resonating within the cavity were extracted through one of the corner mirrors and combined on a photodetector using optical elements. A fringe pattern was formed on the photo-detector by the constructive and destructive interference between the counterrotating light waves. When the RLG was rotated within the plane of the cavity, the fringe pattern translated across the photodetector producing a "beat" frequency.

As predicted by the Sagnac Effect, this beat fre-quency was proportional to the rotation rate by (14:478)

$$\Delta f = \frac{4A}{\lambda P} \Omega \tag{1.1}$$

where

$\Delta f$ = beat frequency between counterrotating beams (Hertz)

$A$ = area enclosed by the gyro (meter$^2$)

$P$ = optical path length of the perimeter of the gyro (meter)

$\lambda$ = laser vacuum wavelength (meter)

$\Omega$ = rotation rate relative to inertial space (radians/sec)
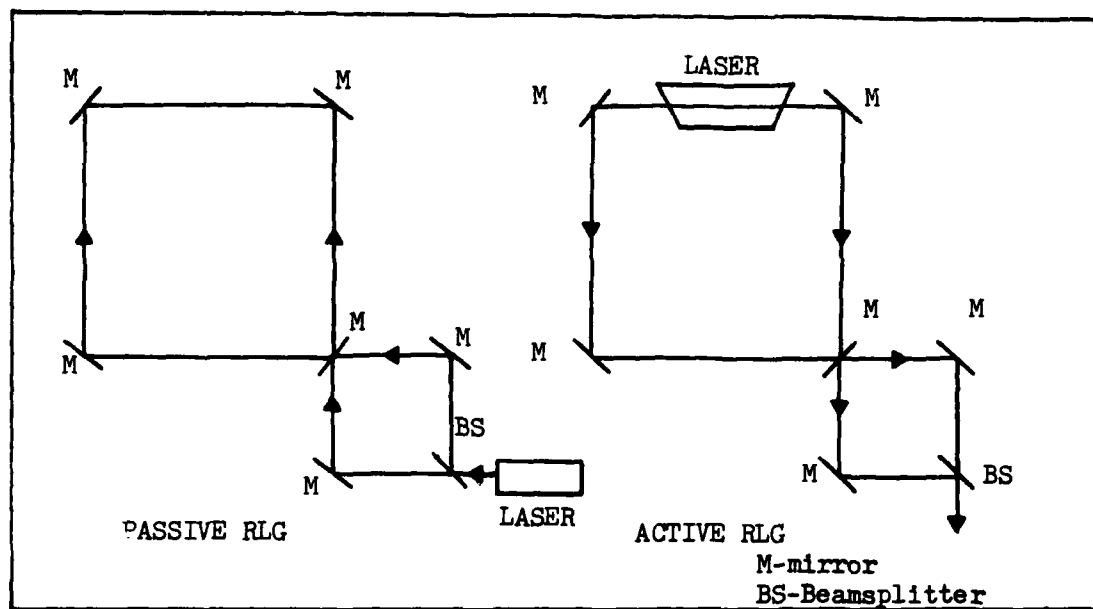
Fig. 1.1. Rosenthal's Proposed Ring Laser Gyros (16:1145)
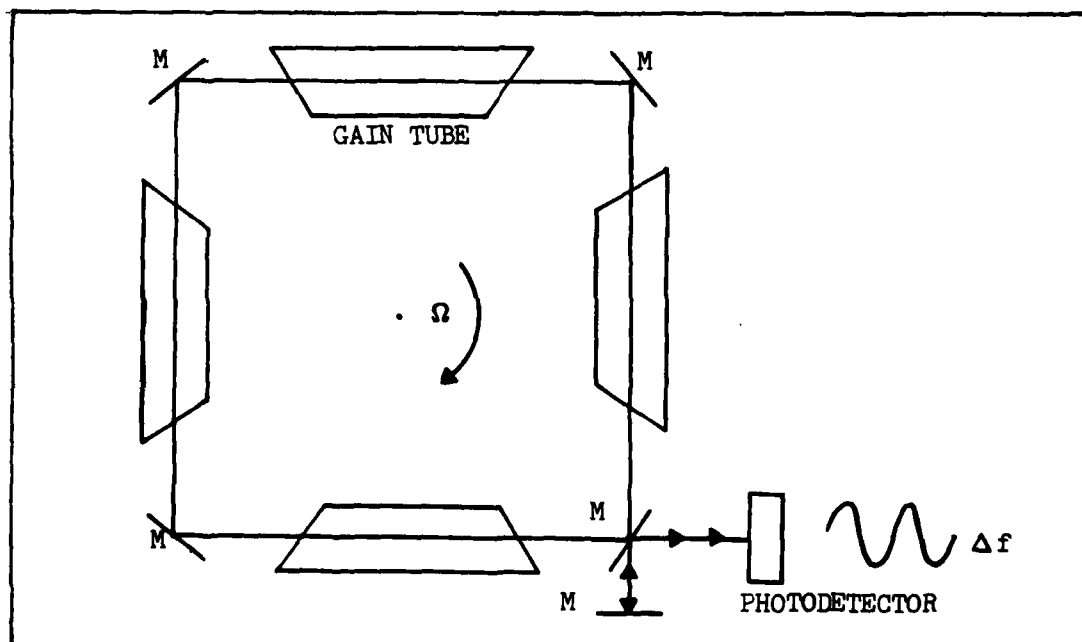


Fig. 1.2. Active Ring Laser Gyro (11:67)

4

The Practical RLG. Since 1963 research in the area of RLGs has resulted in inertial quality performance (drift rates below 0.01 deg/hr), which led to the use of RLGs in the Boeing 757 and 767 aircraft (8:13). The practical RLG still lags behind the capability of the best mechanical gyro, but has many advantages. Requiring no moving parts and needing only a few seconds to warm-up, the RLG has demonstrated a MTBF of over 10,000 hours (19:26). Also, the theoretical limit on precision is better than that of the mechanical gyro (4:14). To achieve high performance, several problems were overcome, as described below.

Because the gain medium is present within the resonant cavity, the clockwise and counter-clockwise beams couple to a common frequency when the gyro is rotated below a rate threshold (1:148). The dominant source of the coupling is the mutual scattering of energy at the mirrors from each of the beams into the direction of the other beam. The result is that, at low rotation rates, there is no frequency difference between the two beams, and so the gyro does not indicate any rotation. This phenomenon is known as lock-in. Figure 1.3 shows a plot of an active RLG output versus input rotation rate.

This problem is resolved through several methods. The most effective one, developed by Honeywell, involves subjecting the gyro to a small cyclical rotation rate, called a dither (19:19), which causes a rotation rate of
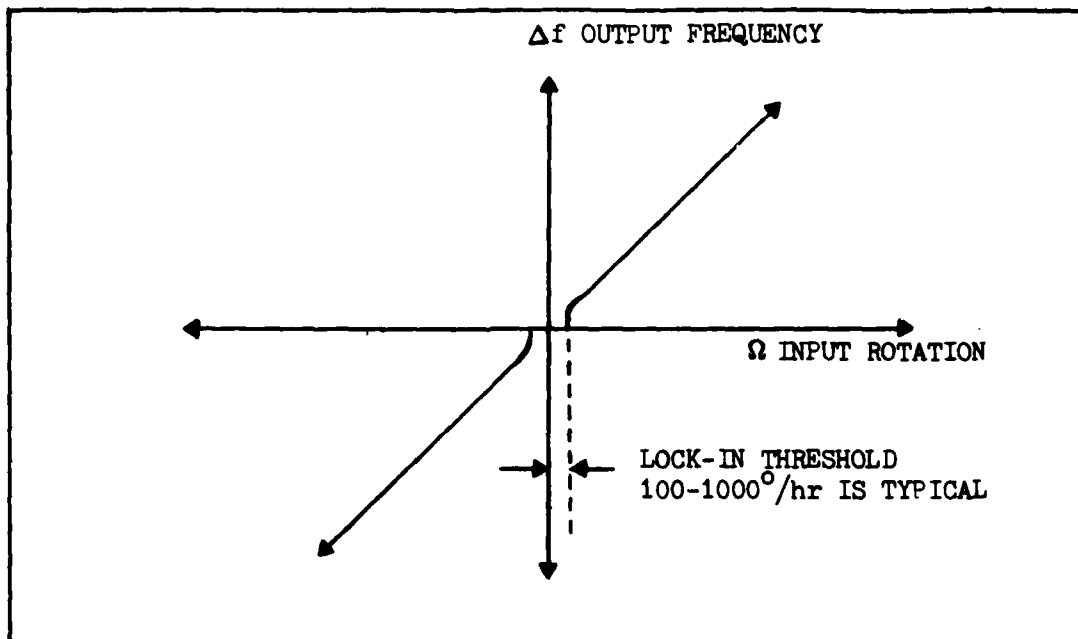
Fig. 1.3. Active RLG Lock-in Effects (1:142)

the gyro above the lock-in threshold. Thus, the gyro remains in the linear portion of the output curve (Figure 1.3). By electronically subtracting out the dither, even rotation rates below the lock-in threshold may be accurately measured.

Although dithering is effective and results in a sensitivity of 0.1 deg/hr, it adds moving parts, induces complexity, injects significant noise sources and makes it impractical to increase the area to perimeter ratio. This and other problems relating to the gain medium being present in resonant cavity, such as multiple lasing modes, discourage the active RLG for use in the geophysical and relativity experiments.

6

Passive RLG. In 1977, Ezekiel and Balsamo pro-
posed and constructed a Passive Resonant Ring Laser Gyro
(PRRLG) based on one of Rosenthal's original designs
(5:478). In this design, the gain medium is not present
within the resonant cavity and so there is no lock-in. In
addition, the passive configuration has the potential to
reach the sensitivities required for the geokinetic and
general relativity experiments because the resonant cavity
can be enlarged without regard to the gain medium as the
PRRLG avoids the multiple mode problem.

## Summary of Current Knowledge (PRRLG)

The configuration demonstrated by Ezekiel and
Balsamo uses a passive resonant cavity and an external
laser to measure the difference between the clockwise and
counter-clockwise optical path lengths of the cavity caused
by inertial rotation. In the scheme shown in Figure 1.4,
the two counterrotating beams are obtained by dividing the
beam with a beamsplitter. The frequency of the external
laser, $f_0$, is shifted to $f_0 + f_1$ by an acousto-optic modu-
lator driven at $f_1$ and to $f_0 + f_2$ by another acousto-optic
modulator driven at $f_2$. As shown in Figure 1.4, feedback
signals to the piezoelectric length transducer lock the
clockwise resonant frequency of the cavity to $f_0 + f_1$
by changing the length of the cavity until maximum intensity
is received by the detector. A second feedback loop locks
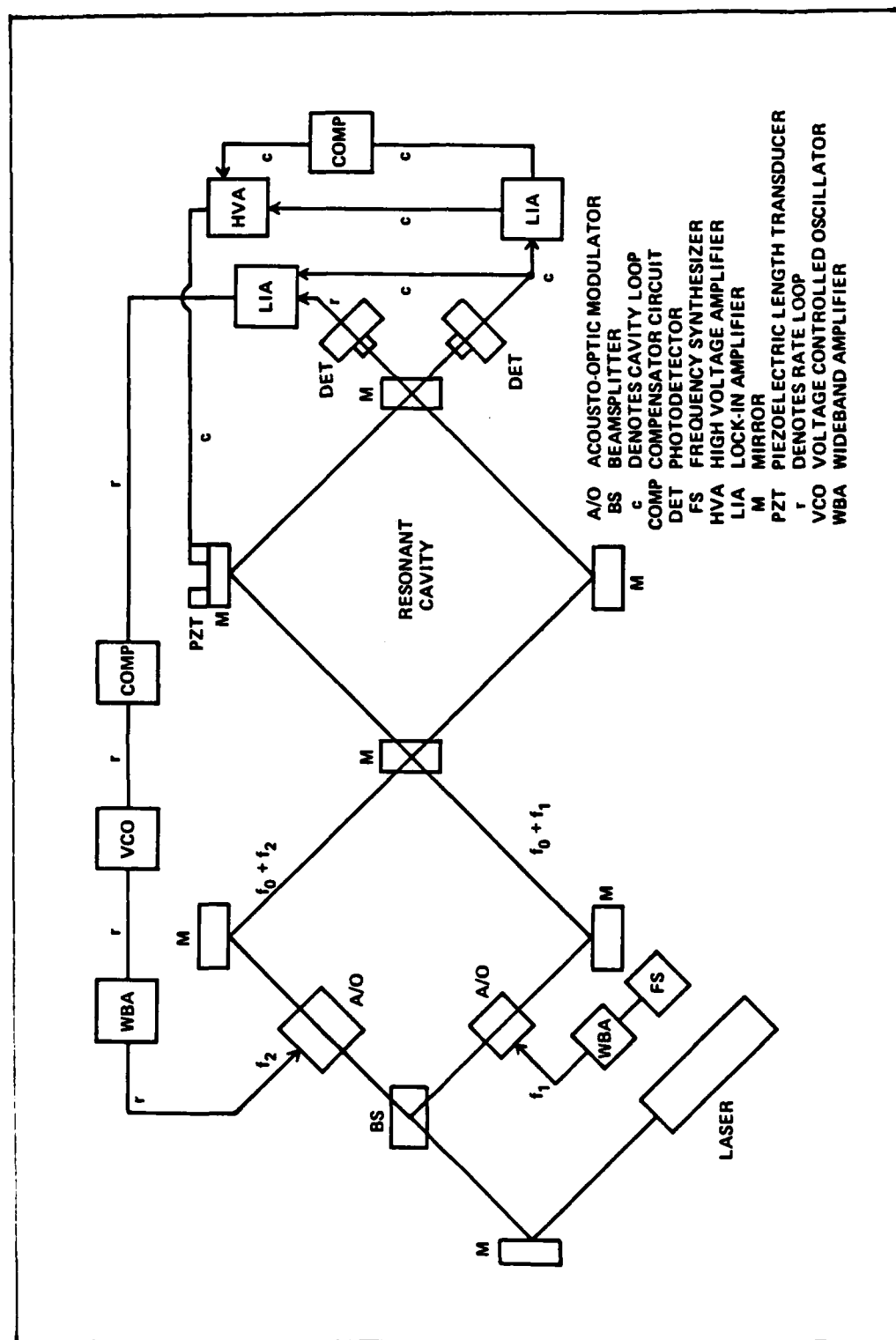
Fig. 1.4. Schematic Diagram of PRRLG (9:19)

Legend:

A/O — ACOUSTO-OPTIC MODULATOR
BS — BEAMSPLITTER
c — DENOTES CAVITY LOOP
COMP — COMPENSATOR CIRCUIT
DET — PHOTODETECTOR
FS — FREQUENCY SYNTHESIZER
HVA — HIGH VOLTAGE AMPLIFIER
LIA — LOCK-IN AMPLIFIER
M — MIRROR
PZT — PIEZOELECTRIC LENGTH TRANSDUCER
r — DENOTES RATE LOOP
VCO — VOLTAGE CONTROLLED OSCILLATOR
WBA — WIDEBAND AMPLIFIER

8

$f_0 + f_2$ to the counter-clockwise resonant frequency of the cavity by adjusting $f_2$ so that maximum intensity is received. Under conditions of no inertial rotation, $f_1$ and $f_2$ are identical; however, with rotation, a frequency difference between $f_1$ and $f_2$ occurs and is proportional to the rotation as given by Equation (1).

Error Sources. Balsamo sponsored two AFIT students, Olkowski and Holland, who built and tested a PRRLG similar to the one shown in Figure 1.4 (9). Their research showed that thermal instability was the greatest source of error. The temperature changes forced the cavity out of alignment and changed the cavity length beyond the control ability of the PZT feedback loop. Other sources of noise were vibration of the cavity mirrors due to platform vibration and air currents, and variation of the index of refraction within the cavity due to air currents. The students recommended using materials with lower thermal coefficients of expansion and an air-tight seal of the resonant cavity.

In 1982, Pugh attempted to eliminate the error sources found by Olkowski and Holland by constructing a PRRLG with a resonant cavity made of Ultra-Low Expansion Quartz (15). Because the mirrors were directly fastened to the cavity and the cavity was partially evacuated, his design negated the errors due to air currents and reduced the thermal instability. Pugh then showed that a major

9

source of error for his configuration was laser intensity variations between the two counterrotating beams, $\Delta I$. The intensity variation caused an error in locking the frequency of the counter-clockwise beam to the cavity. The locking error was, in turn, integrated by the PRRLG, thus causing long-term bias drifts.

In 1983, Nelson built and tested two configurations of the PRRLG using a high quality resonant cavity (12). One configuration was set-up so that the transmitted intensities of the two beams were monitored by photo-detectors. The other configuration allowed for monitoring of the reflected laser intensity from the input mirrors rather than the transmitted intensity. The second method showed how the intensities of the two beams could be equalized by adjusting the amplitude of the signal driving the acousto-optic modulator, thus eliminating most of the long-term bias drift. In addition, the second method resulted in a threefold increase in the sensitivity to rotation over the first method.

## Problem Statement

In previous designs resonance was induced and main-tained by varying the optical path length of the resonant cavity. This was accomplished by using feedback electronics to control a PZT mounted on one or more of the cavity mirrors. Extrapolation of the path length control method

to the large, high quality cavities required for high sensi-
tivities shows a significant drawback related to "linewidth."

Cavity vs Laser Linewidth. In previous designs
using low quality cavities, the cavity linewidth (bandwidth
of frequencies in which light will resonate within the
cavity) was considerably broader than the laser linewidth.
Unfortunately, in dealing with high quality cavities, the
cavity linewidth is narrower than linewidths of commer-
cially stabilized He-Ne lasers. Since this limits perform-
ance of the PRRLG (22) because of the decrease in the
signal-to-noise ratio, it is necessary to develop tech-
niques which narrow the linewidth of the laser for locking
to high quality cavities.

The Frank J. Seiler Research Laboratory is cur-
rently developing a 58 $m^2$ PRRLG which, in theory, will
provide the sensitivities needed to conduct the geokinetic
and relativity experiments (20:117). The configuration
will be similar to those previously described except that,
instead of locking the resonant cavity to the laser, the
laser's frequency will be locked to a resonant mode of the
large cavity. A higher degree of sensitivity is expected
because the signal-to-noise ratio will improve, but the
laser linewidth must be reduced to less than the cavity
linewidth. Fortunately, a laser stabilization technique
has been recently reported by Dr. J. L. Hall, who

11

demonstrated a sub-100 Hz linewidth by locking the laser to low quality resonant cavities (2:97).

Research.  This research is targeted at developing the techniques for locking a He-Ne laser to a small, high quality, thermally stable Cer-vit passive resonant cavity. With the laser stabilized to the resonant frequency of the cavity, the configuration will be modified to act as a PRRLG.

## Method of Approach

The design and assembly of the PRRLG is dictated by the physical characteristics of the components readily available.  The Cer-vit cavity is the dominant factor since its size and the focal length of the mirrors affixed to the cavity are decisive factors in determining the setup geometry and overall dimensions.

First, a frequency stabilized He-Ne laser is locked to the passive cavity.  The energy reflected off the input mirror drives a controller which keeps the frequency of the laser locked to the resonant frequency of the cavity.  The controller varies the laser discharge current (fast loop) or varies the current through a heater coil wrapped around the laser (slow loop with larger dynamic range).  Together, these two loops vary the frequency of the laser by several megahertz and compensate for changes in cavity optical

path length due to rotation or thermal expansion. The beam is, therefore, kept in resonance with the cavity.

This design mode matches the Gaussian beam of the frequency stabilized laser to the mode supported by the cavity. Two cylindrical lenses are precisely placed between the laser and the input mirror so that the laser beam matches the cavity mode.

The components are then mounted on an "Invar" base and aligned. Acousto-optic transducers are placed between the laser and input mirror to isolate the plasma tube from the resonant cavity, thereby eliminating lock-in effects. Measurements verify cavity linewidth and proper operation of the control loop.

The above configuration is then modified to operate as a PRRLG. The laser beam is split and the two beams are injected into the cavity so that one travels clockwise and the other travels counter-clockwise. The control loop to keep the counter-clockwise beam locked to the cavity remains as described above while a secondary loop keeps the clockwise beam locked to the cavity using an acousto-optic modulator. The rotation rate is found by differencing the frequencies added by the acousto-optic modulators.

Evaluation. Tests are conducted by subjecting the PRRLG to the vertical component of earth rate and observing

the frequency difference averaged over each one second
sample period. Assuming ergodicity, the mean and variance
of the frequency difference over the entire test is calcu-
lated to determine sensitivity. Error sources are identi-
fied and minimized.

## Scope

The scope of this research is limited to the design,
fabrication, testing and evaluation of the laser-stabilized
PRRLG. The resonant cavity and the unstabilized laser are
treated as completed components. The design emphasizes the
laser stabilization servos and the mode matching technique.
Major error sources are identified and eliminated as time
and equipment permit.

## Order of Presentation

The introduction presents a general background in
the field of rotation sensing and specifically concentrates
on the development of active and passive RLGs. Chapter II
develops the supporting theory behind the operation of the
PRRLG. The chapter is divided into subsections to deal
with optical cavities, laser principles, the Gaussian beam,
acousto-optic devices, and the Sagnac effect. Chapter III
presents the design and construction of the laser frequency
stabilizer and the PRRLG. Chapter IV discusses the results
obtained from testing the PRRLG and presents the data

collected.  Chapter V discusses the conclusions and gives
recommendations for future investigations.

## II. Theory

This chapter presents the supporting theory for the PRRLG. The first section develops the concept of resonance within an optical cavity and defines several characteristics of optical cavities. Lasing principles are related to methods of controlling the laser frequency. The next section deals with the characteristics of the output of the laser and describes how the beam propagates. The fourth section describes acousto-optic modulators and their function in the PRRLG. The last section derives the Sagnac effect.

### Optical Cavities

An optical cavity is a combination of mirrors or optical devices positioned so that light input into the cavity travels a closed path. A simple optical cavity is the Fabry-Perot interferometer, Figure 2.1, which consists of two highly reflective mirrors placed parallel to each other a distance l apart. If the index of refraction of the medium between the mirrors is "n," the optical path length between the two mirrors is $L = nl$. As shown in the figure, light is incident on the cavity at Mirror A at an angle $\phi$ with respect to the perpendicular to the mirror. Depending on the reflectivity of the mirror, a portion of
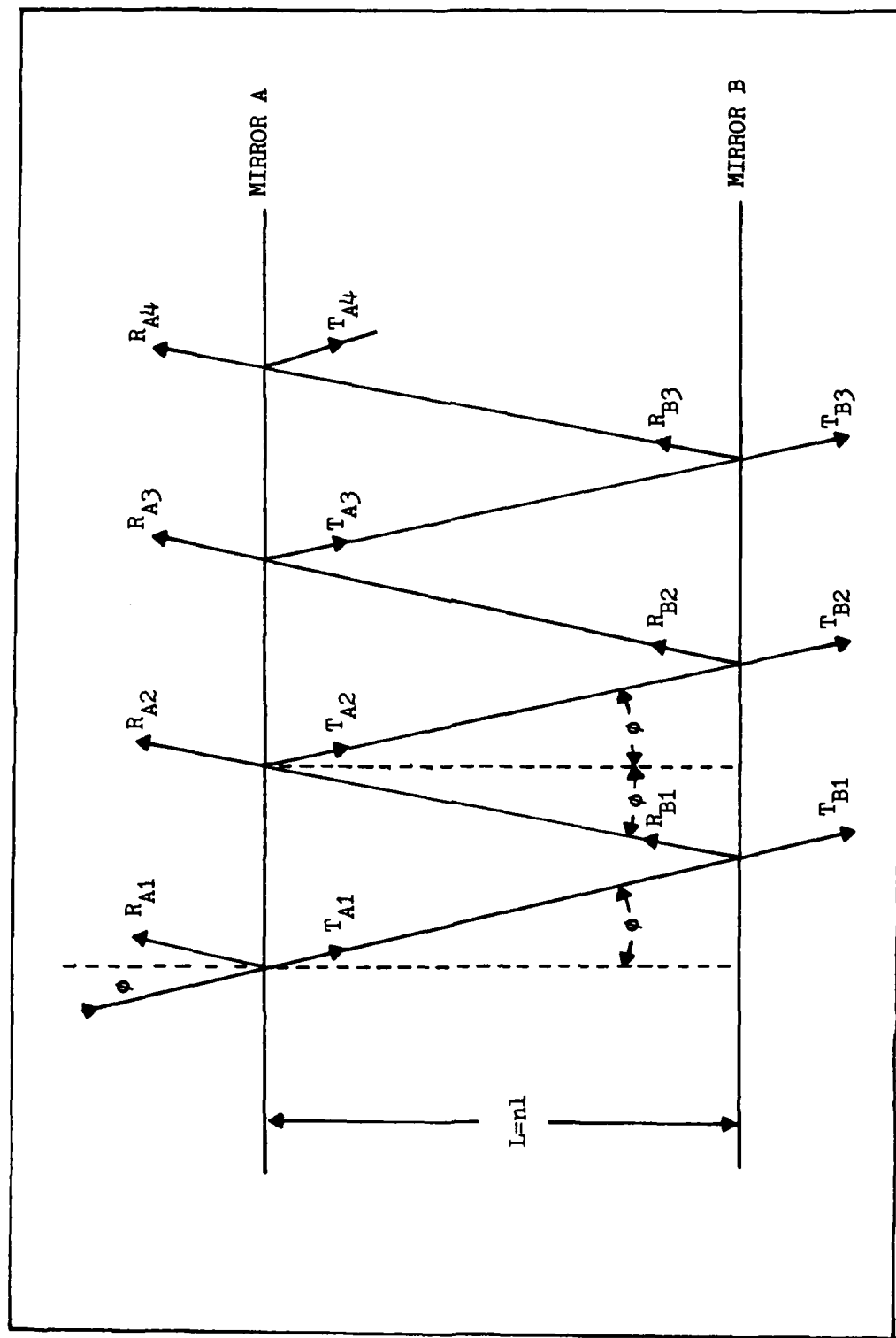
Fig 2.1. Fabry-Perot Interferometer (25:52)

the light is reflected off Mirror A $(R_{A1})$ and a portion is transmitted through the mirror $(T_{A1})$. The light then propagates to Mirror B where, again, depending on its reflectivity, a portion of the light energy is transmitted through Mirror B $(T_{B1})$ and a portion is reflected back to Mirror A $(R_{B1})$. This process continues until the cavity and mirror losses cause the amplitude of the beam within the cavity to go to zero.

Generally, a phase difference is present between the beam just entering the cavity and the partial transmission through Mirror A, $T_{A1}$. This phase difference $\delta$, is given by (25:52)

$$\delta = \frac{4\pi L \cos \phi}{\lambda} \tag{2.1}$$

where $\lambda$ is the wavelength of the light. The result of the phase difference is that the partial reflections $(R_{Ai})$ interfere with each other and the partial transmissions $(T_{Bi})$ interfere with each other. It follows that the summation of the intensities of these partial reflections and transmissions $(I_r$ and $I_t$, respectively) is a function of the phase difference. The fraction of the incident intensity $(I_i)$ that is reflected off Mirror A can be shown (23:116) to be:

$$\frac{I_r}{I_i} = \frac{4(R_A R_B)^{\frac{1}{2}} \sin^2 (\delta/2)}{[1-(R_A R_B)^{\frac{1}{2}}]^2 + 4(R_A R_B)^{\frac{1}{2}} \sin^2 (\delta/2)} \tag{2.2}$$

18

where $R_A$ and $R_B$ are the reflectivities of mirrors A and B, respectively. Likewise, the transmitted fraction of the incident intensity can be shown (23:116) to be:

$$\frac{I_t}{I_i} = \frac{(1-R_A)(1-R_B)}{[1-R(R_A R_B)^{\frac{1}{2}}]^2 + 4(R_A R_B)^{\frac{1}{2}}\sin^2(\delta/2)} \qquad (2.3)$$

When the phase difference is a multiple of $2\pi$, the light intensity transmitted through the cavity is maximized and the light intensity reflected off the input mirror, A, is minimized. Using Equation (2.1) with $\phi = 0$, this occurs when the optical round trip length of the cavity, 2L, is an even number of wavelengths:

$$2L = m\lambda \qquad (2.4)$$

where $\lambda$ is the wavelength of the light and m is an integer. When this condition is satisfied, the light is said to be in resonance with the cavity.

Generally, the resonance condition is expressed in terms of the frequency of the light rather than its wavelength. Since $c/f = \lambda$, where f is the frequency in Hz and c is the speed of light, the resonance condition becomes

$$f = \frac{mc}{2L} \qquad (2.5)$$

Frequencies which are multiples of c/2L are called resonant frequencies of the cavity.

19

Figure 2.2 shows a graph of the fraction of the incident intensity transmitted through the Fabry-Perot interferometer as a function of frequency. As shown, the resonant peaks occur at frequencies which are multiples of c/2L (The same plot could be presented for the reflected intensity where, instead of peaks, there would be valleys). The separation (c/2L) between the resonant peaks defines the Free Spectral Range (FSR) of the cavity, or

$$FSR = c/2L \qquad\qquad (2.6)$$
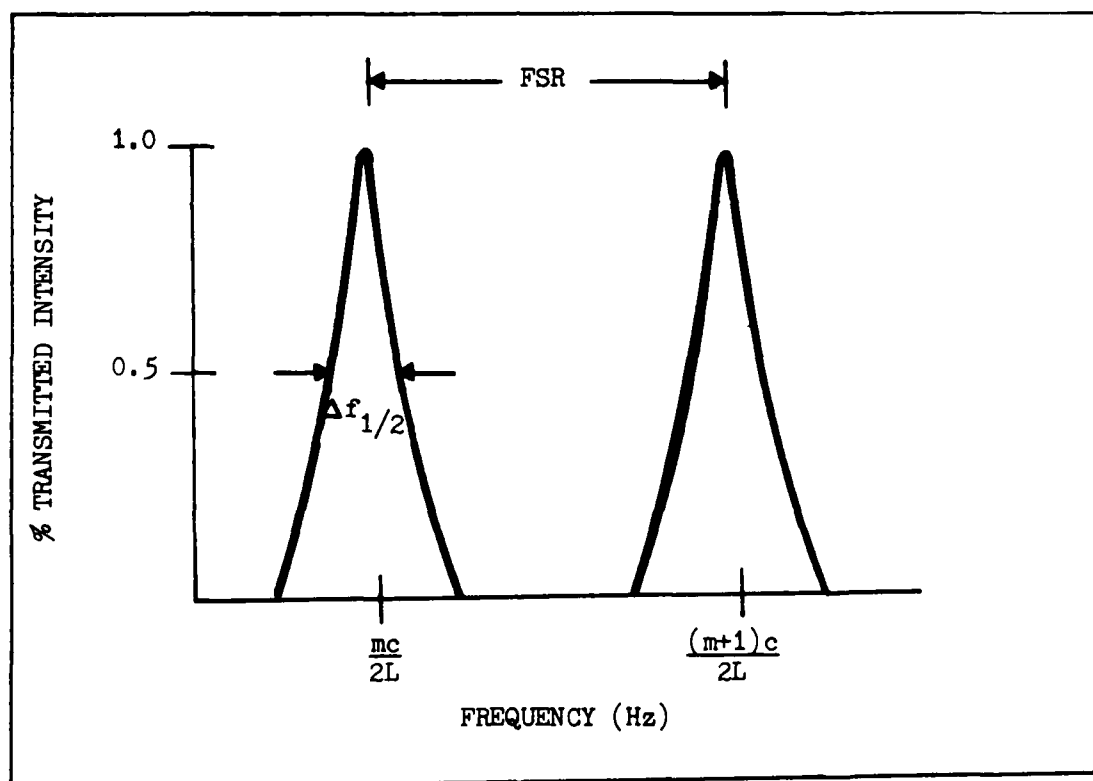
Fig. 2.2.  Cavity Transmitted Intensity
versus Light Frequency

The values of the phase difference which yield a transmission of 1/2 incident intensity can be found as before. These values occur when (23:117)

$$\sin^2(\delta/2) = \frac{[1-(R_A R_B)^{\frac{1}{2}}]^2}{4(R_A R_B)^{\frac{1}{2}}} \tag{2.7}$$

or

$$\sin(\delta/2) = \pm \frac{[1-(R_A R_B)^{\frac{1}{2}}]}{2(R_A R_B)^{\frac{1}{2}}} \tag{2.8}$$

The frequencies corresponding to the 1/2 transmitted intensity values can be shown (23:118) to be

$$f_{\frac{1}{2}} = \frac{c[1-(R_A R_B)^{\frac{1}{2}}]}{4\pi L (R_A R_B)^{\frac{1}{4}}} \tag{2.9}$$

and

$$-f_{\frac{1}{2}} = - \frac{c[1-(R_A R_B)^{\frac{1}{2}}]}{4\pi L (R_A R_B)^{\frac{1}{4}}} \tag{2.10}$$

A characteristic of cavities based on these half transmissions points, called the linewidth of the cavity or the Full Width of Half Maximum (FWHM), is defined by (23:118):

$$\Delta f_{\frac{1}{2}} = f_{\frac{1}{2}} - (-f_{\frac{1}{2}})$$

$$= \frac{c}{2L} \frac{1-(R_A R_B)^{\frac{1}{2}}}{\pi (R_A R_B)^{\frac{1}{4}}} \tag{2.11}$$

21

From this expression for the linewidth of the cavity and the expression in Equation (2.6), the finesse (F) of the cavity is determined (23:119):

$$F = \frac{FSR}{\Delta f_{\frac{1}{2}}} = \frac{\pi (R_A R_B)^{\frac{1}{4}}}{1 - (R_A R_B)^{\frac{1}{2}}} \qquad (2.12)$$

The finesse gives the number of linewidths that would fit into one FSR. The finesse can also be considered a measure of the resolving power of the cavity, that is, its ability to resolve one frequency of light from another within the same FSR.

The light energy between the two mirrors builds up over time until an equilibrium point between input intensity and output intensity is reached. Similarly, it takes time for the intensity to decay to zero after the external light source is shut off. The decay time is known as the photon lifetime ($\tau_c$). If cavity losses are predominantly due to the transmission of light energy, the photon lifetime is (25:68):

$$\tau_c = \frac{L}{c[1 - (R_A R_B)^{\frac{1}{2}}]} \qquad (2.13)$$

which redefines the cavity finesse as (25:68):

$$F = \frac{\pi c \tau_c}{L} \qquad (2.14)$$

22

The concepts for the Fabry-Perot interferometer shown in Figure 2.1 can easily be extended to a more complex cavity. A square cavity, for example, would have four mirrors with $R_A$, $R_B$, $R_C$ and $R_D$ as their respective reflectivities. The optical round trip path length is the index of refraction of the medium multiplied by the perimeter of the cavity (P)

$$P = np \qquad (2.15)$$

From this, the transmitted fraction of the incident intensity for a beam in resonance, as taken from Equation (2.3), is

$$\frac{I_t}{I_i} = \frac{(1-R_A)(1-R_C)}{[1-R_A R_B R_C R_D)^{\frac{1}{2}}]} \qquad (2.16)$$

This yields resonant frequencies of

$$f = \frac{mc}{P}$$

with the

$$FSR = c/P \qquad (2.17)$$

Similarly, the cavity linewidth, cavity finesse, and photon lifetime corresponding to Equations (2.11), (2.12) and (2.13), respectively are:

23

$$\Delta f_{\frac{1}{2}} = \frac{c}{P} \frac{1-(R_A R_B R_C R_D)^{\frac{1}{2}}}{\pi (R_A R_B R_C R_D)^{\frac{1}{4}}} \qquad (2.18)$$

$$F = \frac{\pi (R_A R_B R_C R_D)^{\frac{1}{4}}}{1-(R_A R_B R_C R_D)^{\frac{1}{2}}} \qquad (2.19)$$

$$\tau_c = \frac{P}{c[1-(R_A R_B R_C R_D)^{\frac{1}{2}}]} \qquad (2.20)$$

## Laser Fundamentals

A laser consists of three basic components: a gain medium, a pumping mechanism to excite the gain medium, and a resonant optical cavity (13:51-76). The frequency of the laser beam is due to the selection of the gain medium and the selection of the distance between the two cavity mirrors.

The gain medium most often used in ring laser gyros is Helium-Neon gas. An electrical discharge through the gas acts as a pumping mechanism for the laser. The electrons from the current applied to the laser collide with the Helium atoms, raising them to a higher energy state. Through collisions, the Helium atoms give up their stored energy to the Neon atoms, which raises the Neon atoms to a higher energy state ($E_1$). If left alone, the Neon atoms return to their ground state ($E_0$) by themselves,

24

releasing a photon exhibiting a wavelength of about 632.8 nonometers (nm). When Neon atoms release photons in this manner, spontaneous emission occurs.

The Neon atoms can also return to the ground state by being stimulated by another photon. During this process of stimulated emission, the photon released by the Neon atom has the same phase and direction as the photon that originally stimulated the atom. The result is two photons traveling in the same direction, exhibiting the same wavelength and phase (see Figure 2.3).
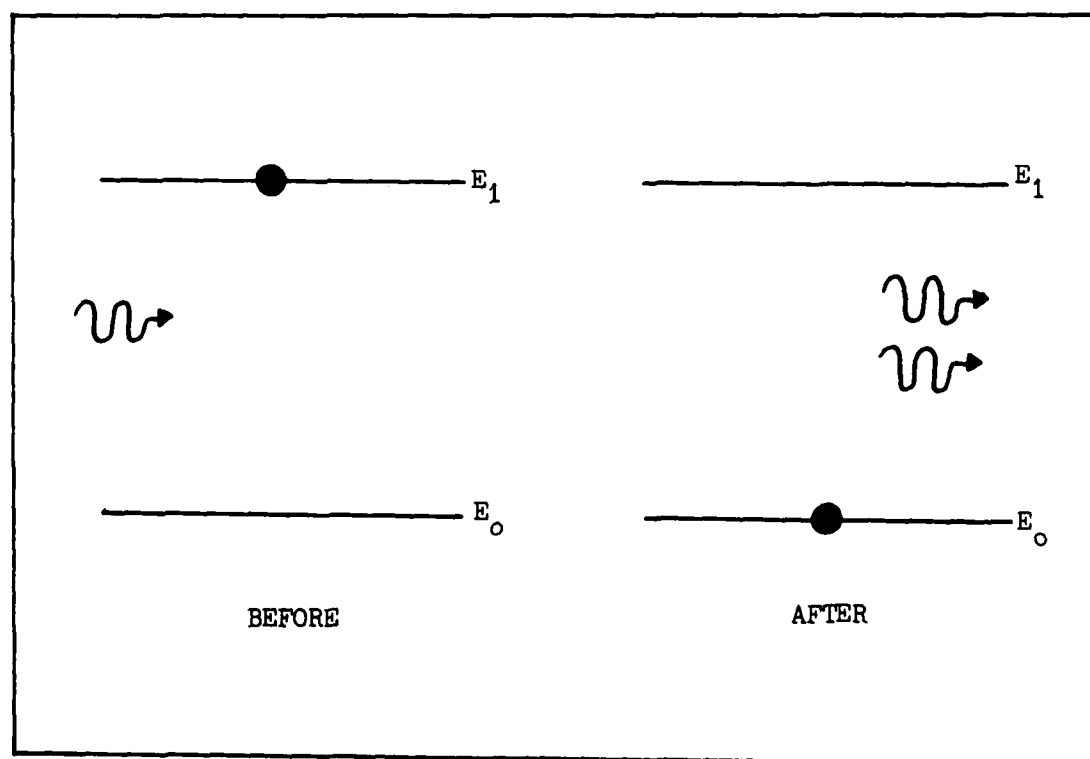
Fig. 2.3. Stimulated Emission of a Photon (13:56)

25

By placing two mirrors on either side of the gain medium, a resonant cavity can be constructed. When a photon emitted from a Neon atom strikes one of the mirrors so that it is reflected directly back into the gain medium, a chain reaction is set up. The photon travels back through the medium and stimulates many other high energy state Neon atoms to give off a photon traveling in the same direction and exhibiting the same phase as the original photon. These photons, in turn, stimulate more Neon atoms to give up a photon. The end result is that a majority of the photons are traveling back and forth between the two mirrors. If the number of photons emitted during a single pass through the gain medium is greater than the number of photons absorbed or lost due to cavity losses, then lasing occurs. Lasing continues as long as there are sufficient excited Neon atoms to produce a gain higher than cavity losses. In the He-Ne laser, the lasing stabilizes at a point when the pumping mechanism is replenishing upper state Neon atoms at the same rate the lasing process and other loss mechanisms are depleting them.

As shown in Figure 2.4, the gain medium produces gains greater than the cavity losses only for light within a narrow frequency band (from point A to point B). The resonance of the optical cavity further restricts the range of frequencies to be a multiple of the FSR of the cavity, $c/2L$. From this, light at the resonant frequency has

26
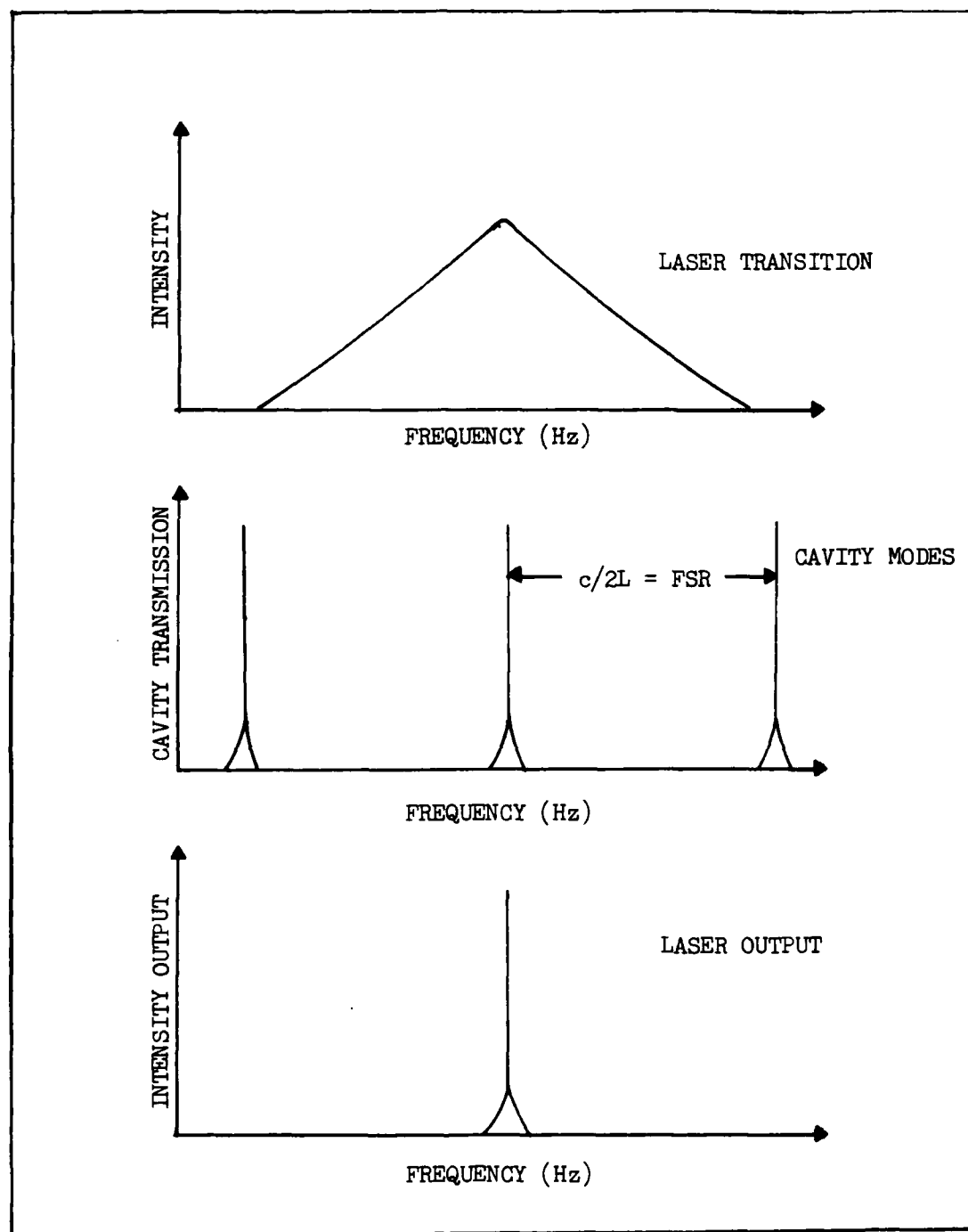
Fig. 2.4.   He-Ne Gain Profile and
            Resonance Condition (13:92)

the lowest cavity losses, and undergoes amplification until it is the only frequency amplified and the non-resonant frequencies die out. The output of the laser is, therefore, the frequency determined by the resonant frequency of the cavity and the laser transition.

A standard method of controlling the frequency of the laser output involves changing the resonance condition of the cavity, by varying the optical path length between the two mirrors (6). This is accomplished by changing the index of refraction or the physical length of the cavity. The index of refraction can be varied by changing the discharge current in the laser. Reducing the discharge current lowers the index of refraction and increasing the discharge current raises the index of refraction. Controlling the physical distance between the mirrors can be accomplished by applying current to a heater coil wrapped around the glass gain tube. This causes the gain tube to expand. With a combination of these two control mechanisms and the proper feedback signals, the laser frequency can be varied to any frequency allowable by the laser transition curve.

## The Gaussian Beam

The output of a laser is a Transverse Electro-Magnetic (TEM) wave. For our experiment the laser beam is circularly symmetric in cross-section, where the intensity

profile of the wave has one peak and gradually tapers to zero in accordance with $\exp\{-(\rho/\omega)^2\}$ where $\rho$ is the distance from the center of the beam and $\omega$ is the spot size. Such a beam, called a Gaussian beam, is shown in Figure 2.5.
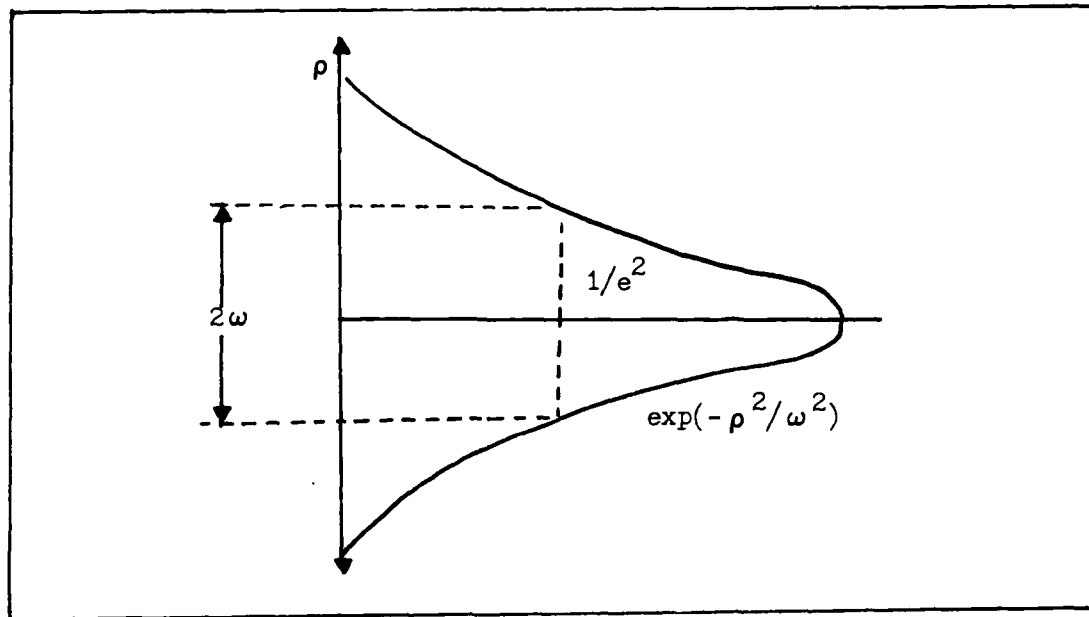


Fig. 2.5.  Gaussian Beam Intensity
Cross-Section (13:16)

The values of $\rho$ for which the beam irradiance decreases to $1/e$ of its value at the center is termed the spot size, $\omega$. In general, $\omega$ will vary from point to point along the axis of the beam.  At one point in the cavity, called the beam waist, the Gaussian beam has its minimum spot size, $\omega_o$, as shown in Figure 2.6.  The spot size of the wave at any point along the beam can be expressed as a function of

29
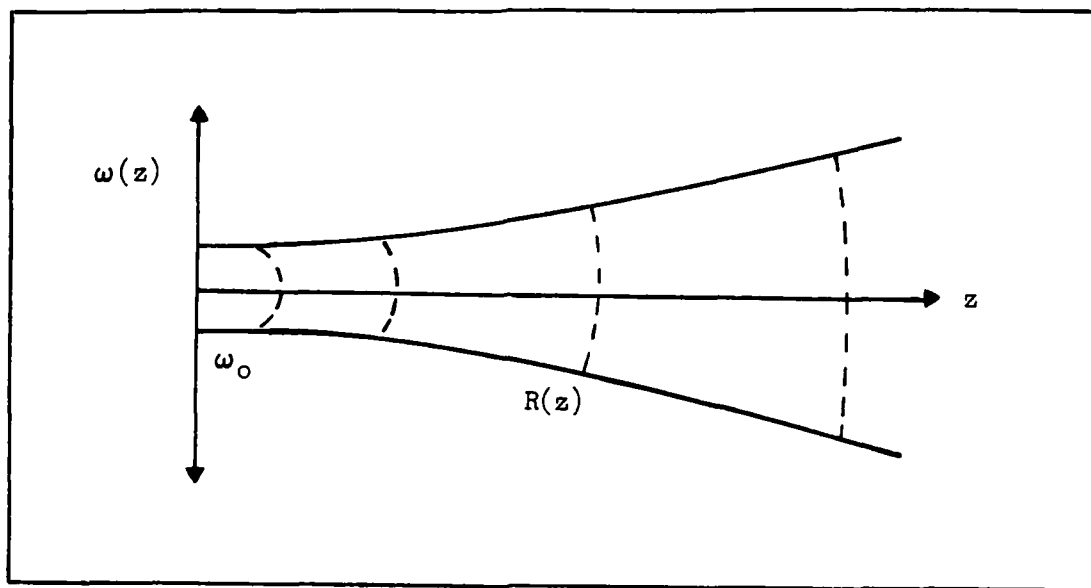
Fig. 2.6.   Propagation of a Gaussian Beam (13:17)

the spot size at the waist and the distance from the waist
(23:60):

$$\omega(z) = \omega_0 = \sqrt{1 + (\frac{\lambda z}{\pi \omega_0})^2} \qquad (2.22)$$

where

$\omega(z)$ = the beam's spot size a distance z from the
   waist

   z = distance from the waist along the beam

$\omega_0$ = spot size at the beam waist

$\lambda$ = wavelength of the laser beam

In addition to having a beam waist, the beam wavefront also
exhibits a radius of curvature.  As the laser propagates,
the divergence of the spot size causes the wavefront to

30

curve (Figure 2.6). The radius of curvature at any point is given by (23:60):

$$R(z) = z[1 + (\frac{\pi\omega_o^2}{\lambda z})^2]$$  (2.23)

where

R(z) = radius of curvature at distance z from the beam waist

At the beam waist, the radius of curvature is infinite since z = 0. With these two parameters the entire Gaussian beam can be characterized at any point along the beam's path.

## Acousto-Optic Modulators

The acousto-optic modulator is a device that can shift the frequency of the incident light by precise amounts by diffracting the light from a traveling sound wave (24). When a modulating voltage is applied to the acousto-optic modulator, a shaker converts the electrical signal to a sound wave that propagates through the acousto-optic crystal. This sound wave induces a strain within the glass which causes the index of refraction of the plate to vary with the wavelength of the acoustic wave. The periodic change in the index of refraction causes the velocity of the optical wavefront to change simultaneously. The end result is that the wavefront is Doppler shifted by multiples of the acoustic wave's frequency.

In acousto-optic applications only the first order beam is used, where the beam is Doppler shifted by the frequency of the sound wave. As shown in Figure 2.7, the first order beam is offset from the zeroth order beam by the Bragg angle given by (24:116):

$$\theta_B = \sin^{-1}\left(\frac{\lambda_o}{2\lambda_s}\right) \qquad (2.24)$$

where

$\theta_B$ is the Bragg angle

$\lambda_o$ is the wavelength of the incident light

$\lambda_s$ is the wavelength of the acoustic wave
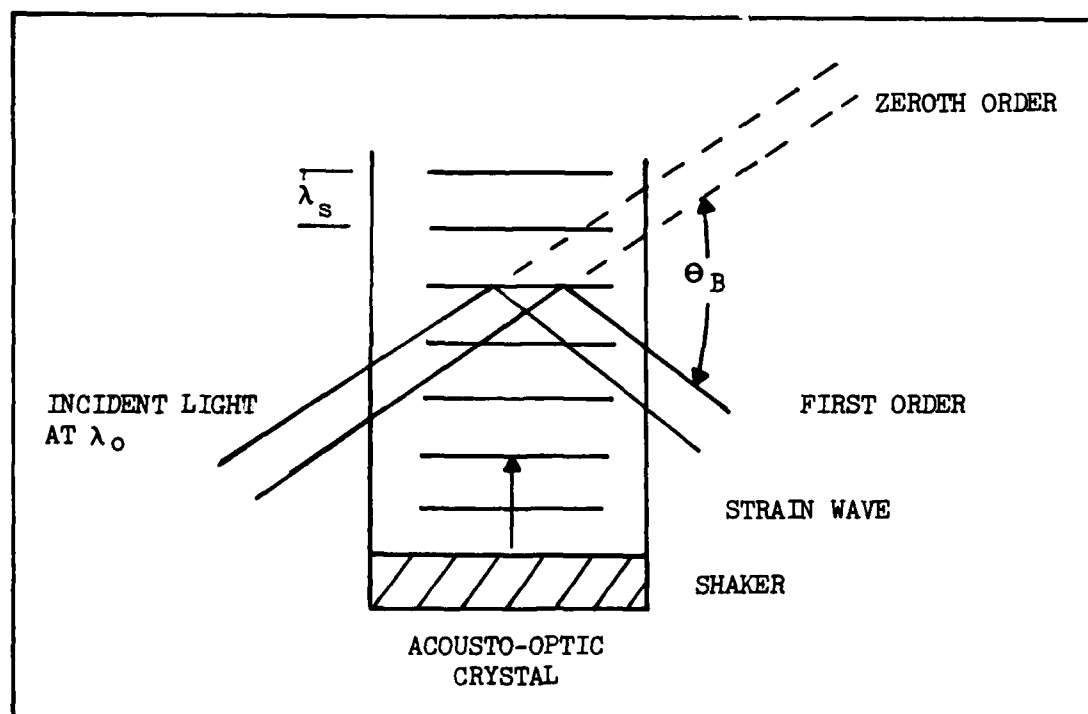


Fig. 2.7.  Acousto-Optic Modulation (24:115)

32

The frequency shifting feature of the acousto-optic modulator (A/O) is used in the RLG to shift the frequency of the unlocked (clockwise) beam by precise amounts to drive the beam into resonance with the cavity. The counter-clockwise beam is frequency shifted by 40 MHz (within the linear range of device) and then injected into the cavity. The laser control loop changes the original frequency of the laser so that the counter-clockwise beam is in resonance with the cavity. Under no rotation and under ideal environmental conditions, the clockwise beam is also in resonance with the cavity. But while rotating, the clockwise beam goes out of resonance due to the Sagnac effect (See Equation (1.1)). To drive that beam back into resonance, a feedback circuit connected to an acousto-optic modulator shifts the frequency of the clockwise beam. The difference between the frequencies driving the A/Os defines the difference frequency in Equation (1.1) used to determine rotation rate.

In addition to varying the frequency of the incident light, the A/O can slightly vary the intensity of the refracted light by varying the amplitude of the modulating signal driving the A/O. The amplitude of this signal determines the intensity of the acoustic wave, which determines the change in the index of refraction in the glass plate. This specifies the amount of light diffracted at each sound wave, which finally determines the intensity of

33

the diffracted light beam. This feature of the A/O is used in the RLG to balance the intensities of the two counter-rotating beams prior to their injection into the resonant cavity.

The acousto-optic modulator also acts to keep the forward light beam from reflecting back into the gain medium. When light is reflected back into the acousto-optic, it is not shifted back to its original frequency or original beam path. Instead the beam is shifted twice in frequency and deflected so that it does not retrace the forward beam path. The net result is that the reflected beam is not aligned to the laser cavity and is not at the resonant frequency of the cavity. Therefore, the mutual coupling between beams as seen in active RLGs is avoided since the light is not fed back into the laser cavity.

## Sagnac Effect

Optical rotation sensors base their measurements on the Sagnac effect, which determines rotation by measuring a difference in the optical path length of two counter-rotating beams (17). This effect can be observed as well as derived by examining an ideal circular interferometer (see Figure 2.8). Light enters the interferometer at point A and is split into a clockwise and a counter-clockwise beam by the beamsplitter. These two beams are, then, constrained to follow the circular path, of radius R,

34
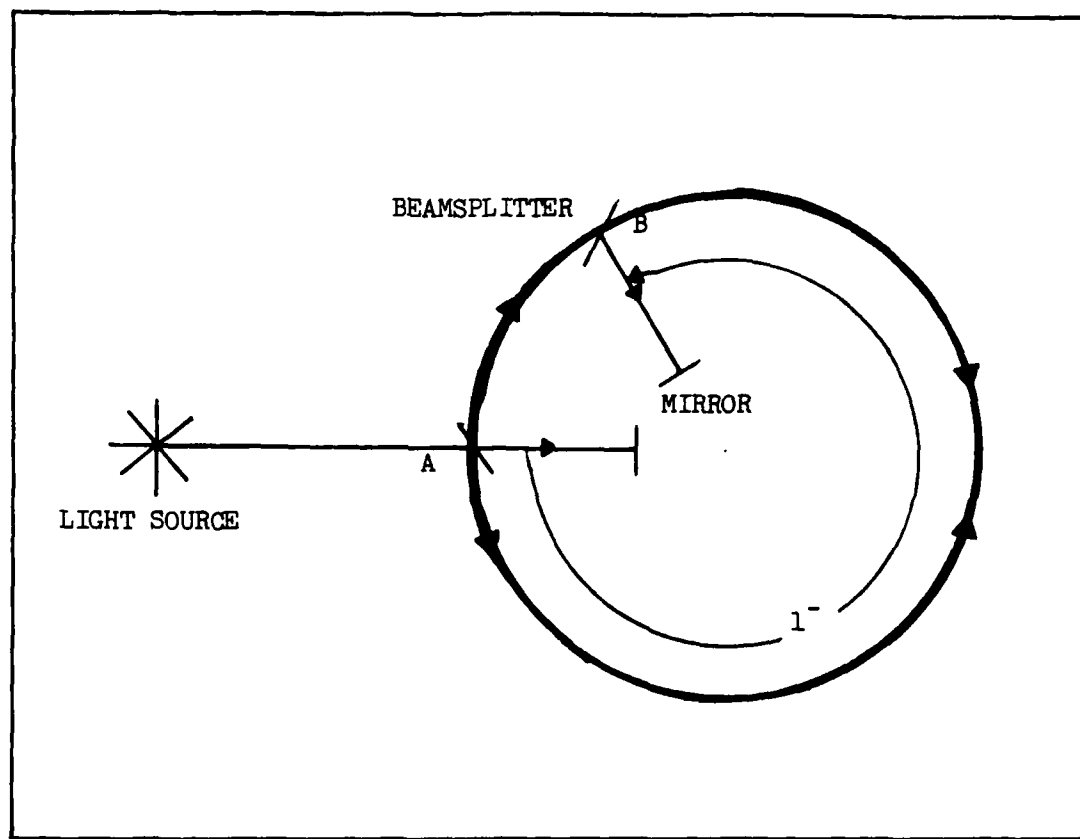
Fig. 2.8. Circular Rotating Interferometer (1:135)

as defined in the figure. Under no inertial rotation, the time for the light traveling in either direction to complete a trip around the interferometer back to point A is

$$t = \frac{2\pi R}{c} \qquad (2.25)$$

where R is the radius of the interferometer, and c is the speed of light (constant).

In the presence of inertial rotation, however, there is a time difference between a counter-clockwise and

35

a clockwise circulation of the light as seen by a sta-
tionary observer. As before, the two beams leave the beam-
splitter at point A. The counter-clockwise beam rotates
in opposition to the direction of rotation and meets the
beamsplitter again at point B instead of point A. Like-
wise, the clockwise beam, traveling in the same direction
as the direction of rotation, meets the beamsplitter at
point B. From Figure 2.8, the distance traveled by the
counter-clockwise beam $l^-$ and the distance traveled by the
clockwise beam $l^+$ is

$$l^- = ct^- = 2\pi R - R\Omega t^- \qquad (2.26)$$

$$l^+ = ct^+ = 2\pi R + R\Omega t^+ \qquad (2.27)$$

where $t^+$ and $t^-$ are, respectively, the time for the clock-
wise and counter-clockwise beams to circulate around the
interferometer (from A to B) and $\Omega$ is the inertial rota-
tion rate. Solving for the time difference between the
two circulations yields:

$$\Delta t = t^+ - t^- = \frac{2\pi R}{c-R\Omega} - \frac{2\pi R}{c+R\Omega}$$

$$= \frac{2\pi R(c+R\Omega) - 2\pi R(c-R\Omega)}{c^2 - (R\Omega)^2}$$

$$= \frac{4\pi R^2}{c^2 - (R\Omega)^2} \, \Omega \qquad (2.28)$$

For the proposed experiments $c^2 >> (R\Omega)^2$, so Equation (2.28) reduces to

$$\Delta t = \frac{4\pi R^2}{c^2} \Omega$$

or if we let A be the area enclosed by the interferometer (14:481)

$$\Delta t = \frac{4A}{c^2} \Omega \tag{2.29}$$

This time difference expression can be converted to a fringe shift expression by using the relationship

$$\Delta Z = \frac{c\Delta t}{\lambda} \tag{2.30}$$

where

$\Delta Z$ = the fringe shift due to inertial rotation

$\lambda$ = the wavelength of the light beam

Thus,

$$\Delta Z = \frac{4\pi R^2}{\lambda c} \Omega = \frac{4A}{\lambda c} \Omega \tag{2.31}$$

assuming that the rotation is normal to the interferometer. The time difference $\Delta t$ is directly proportional to the length difference $\Delta l$ by

$$\Delta l = c\Delta t \tag{2.32}$$

Therefore, the optical path length difference between the two counterrotating beams is (1:137):

37

$$\Delta l = \frac{4A}{c} \Omega \qquad\qquad (2.33)$$

This length difference (typically $10^{-15}$ cm) is not directly measurable. By relating the path length difference to a difference in frequencies of two laser beams resonating within the cavity, the rotation rate can be determined.

The ring containing the light beams can be interpreted as a set of two Fabry-Perot interferometers, one in the clockwise direction and one in the counterclockwise direction. As was shown in the first section, a necessary condition for the light to resonate within the interferometer is $L = m\lambda$ (23:115), where L is the perimeter of the ring, m is an integer, and $\lambda$ is the wavelength of the light. Since $\lambda = c/f$, this equation becomes

$$L = \frac{mc}{f} \qquad\qquad (2.34)$$

Solving for the frequency, f, gives

$$f = \frac{mc}{L} \qquad\qquad (2.35)$$

By taking the derivative of this equation with respect to L, we can relate the difference in optical path length, $\Delta L$, to a difference in the resonant frequencies of the interferometers.

$$\frac{\partial f}{\partial L} = - \frac{mc}{L^2}$$

$$\partial f = - \frac{mc}{L^2} \partial L \tag{2.36}$$

Assuming $\partial L$ and $\partial f$ to be small, then Equation (2.36) becomes

$$\Delta f = - \frac{mc}{L^2} \Delta L \tag{2.37}$$

Substituting $L = m\lambda$ for one of the values of L results in

$$\Delta f = - \frac{c}{L\lambda} \Delta L \tag{2.38}$$

Finally substituting Equation (2.33) for $\Delta L$ in Equation (2.38) gives (1:138):

$$\Delta L = - \frac{4A}{\lambda P} \Omega \tag{2.39}$$

which relates the difference in the resonant frequencies, $\Delta f$, for the two interferometers to the inertial rotation, $\Omega$, of the ring. This equation forms the basis upon which optical rotation sensors derive their measurements.

III.　Experiment Design and Setup

The concepts developed for the PRRLG are now imple-
mented.　The laser is frequency stabilized to the cavity
reference frequency using the feedback control loop
described in the second section.　This design is augmented
as shown in the third section to yield a PRRLG consisting
of the laser frequency and secondary control loops which
keep the counterrotating beams in resonance with the
cavity.

## Cavity Description

As shown in Figure 3.1, the cavity used for this
experiment consists of a square block of Cer-vit with holes
bored through the block to define the path of the laser
beam.　The low coefficient of thermal expansion of Cer-vit,
$0.22 \times 10^{-6}$ cm/cm/deg C, makes this cavity 100 times more
thermally stable than cavities used in previous experiments
(5; 12; 15; 18).　The cavity is also evacuated to $5.8 \times 10^{-8}$
Torr to minimize both scattering and the effect of air cur-
rents within the cavity.

To contain and focus the laser beam within the
cavity, four high quality mirrors are used.　Affixed on
opposing corners of the cavity are flat input mirrors with
a reflectivity of 99.997 percent.　Two spherical mirrors
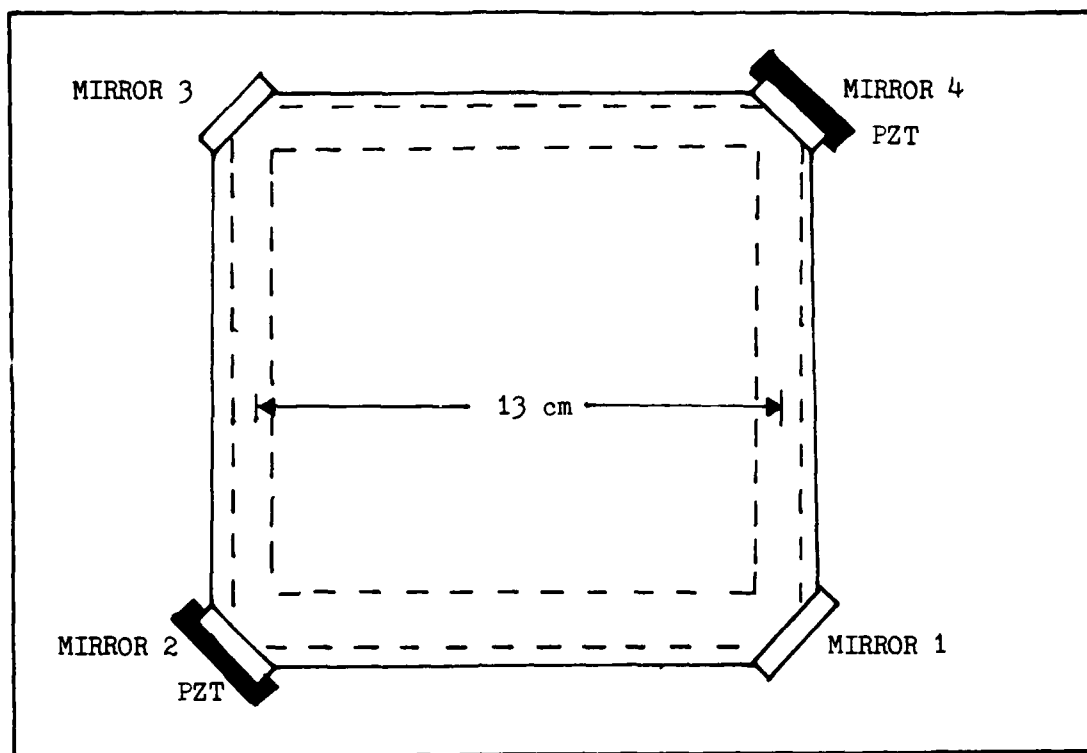
Fig. 3.1. Resonant Cavity

each with a radius of curvature of 800 cm and reflectivity
of 99.9998 percent are affixed on the other opposing
corners. Table 3.1 shows the cavity parameters calculated
from Equations 2.17 - 2.20 (lossless cavity assumed).

## Laser Stabilization

For this experiment, frequency stabilization of
a 1 milliwatt, single-mode, He-Ne laser was performed by
controlling the optical length of the laser cavity with two
control circuits for the laser gain tube (6). By con-
trolling the optical length of the gain tube, the resonant

41

TABLE 3.1

RESONANT CAVITY PARAMETERS

| | |
|---|---|
| Free Spectral Range (FSR) . . . . . . . . . . . . | 576.92 MHz |
| Cavity Linewidth ($\Gamma$) . . . . . . . . . . . . . . | 5876 Hz |
| Cavity Finesse (F) . . . . . . . . . . . . . . | 98,182 |
| Cavity Lifetime ($\tau_c$) . . . . . . . . . . . . . | 54 sec |

condition of the laser cavity can also be controlled. A
schematic diagram of these two circuits is shown in
Figure 3.2. One circuit controls the discharge current and,
therefore, the index of refraction within the gain tube.
The second circuit uses heat to control the physical dis-
tance between the two laser mirrors.

Control Circuits. The discharge current control
circuit provides a high speed (bandwidth of about 50 KHz)
control of the laser's frequency (100 KHz per volt applied).
This circuit alone does not provide enough dynamic range
for the laser to remain locked for more than several
minutes and, thus, is complimented by a low bandwidth con-
troller.

The lower frequency control loop (bandwidth of
about 20 Hz) consists of heater tape wrapped around the
gain tube. When a voltage is applied to the heater tape,
thermal energy proportional to the voltage drop across the
100 ohm heater is produced. This heat subsequently causes

42
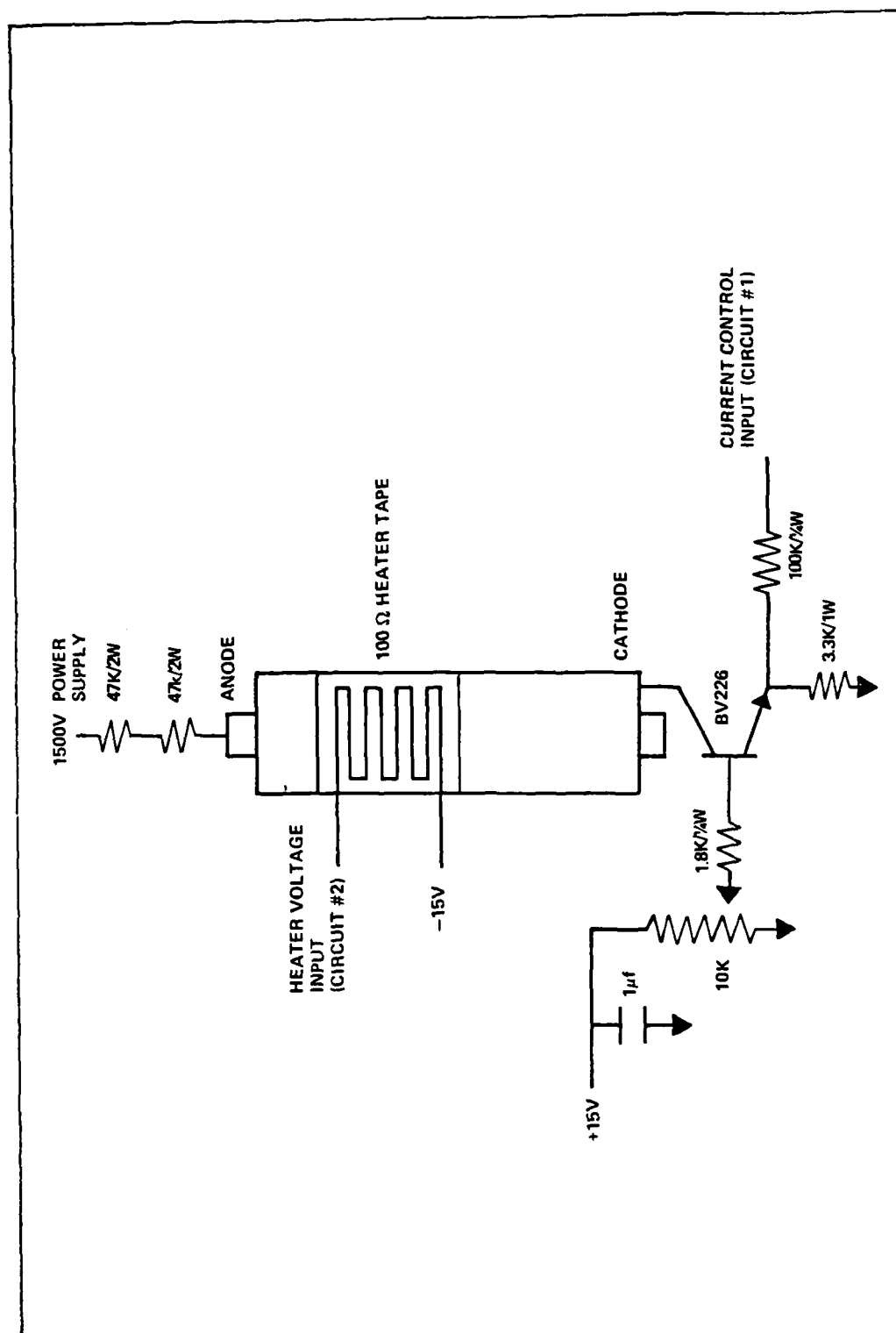
Fig. 3.2. Laser Frequency Control Circuits

thermal expansion of the glass tube so that the distance between the laser mirrors is increased. So that negative and positive length changes can be made, a bias is added to the control voltage. In this manner, the heater loop changes the laser's frequency by approximately 100 MHz per volt applied to the heater, thus providing the greater dynamic range needed to remain locked to the resonant cavity for indefinite lengths of time.

Setup. As shown in Figure 3.3, tests to observe the performance of the laser frequency stabilizer are set up so that the optics are consistent with those required for the PRRLG. The polarization of the laser light is aligned to the S-polarization of the resonant cavity by sending the beam through a half wave plate ($\lambda/2$). Two cylindrical lenses then focus the laser beam to match it to the Transverse Electromagnetic ($TEM_{0,0}$) mode of the cavity. Details of the mode-matching procedure are contained in Appendix A. Before the laser beam is injected into the resonant cavity, an acousto-optic modulator (A/O) shifts the frequency of the beam $f_0$ by a constant frequency $f_1$. In addition, the A/O serves to prevent energy from being directed back into the laser gain tube, thus avoiding lock-in problems. A flat corner mirror, $M_5$, and a translational stage (consisting of a thick glass plate mounted at an angle offset from the normal to the beam) then directs the beam into the cavity.

44
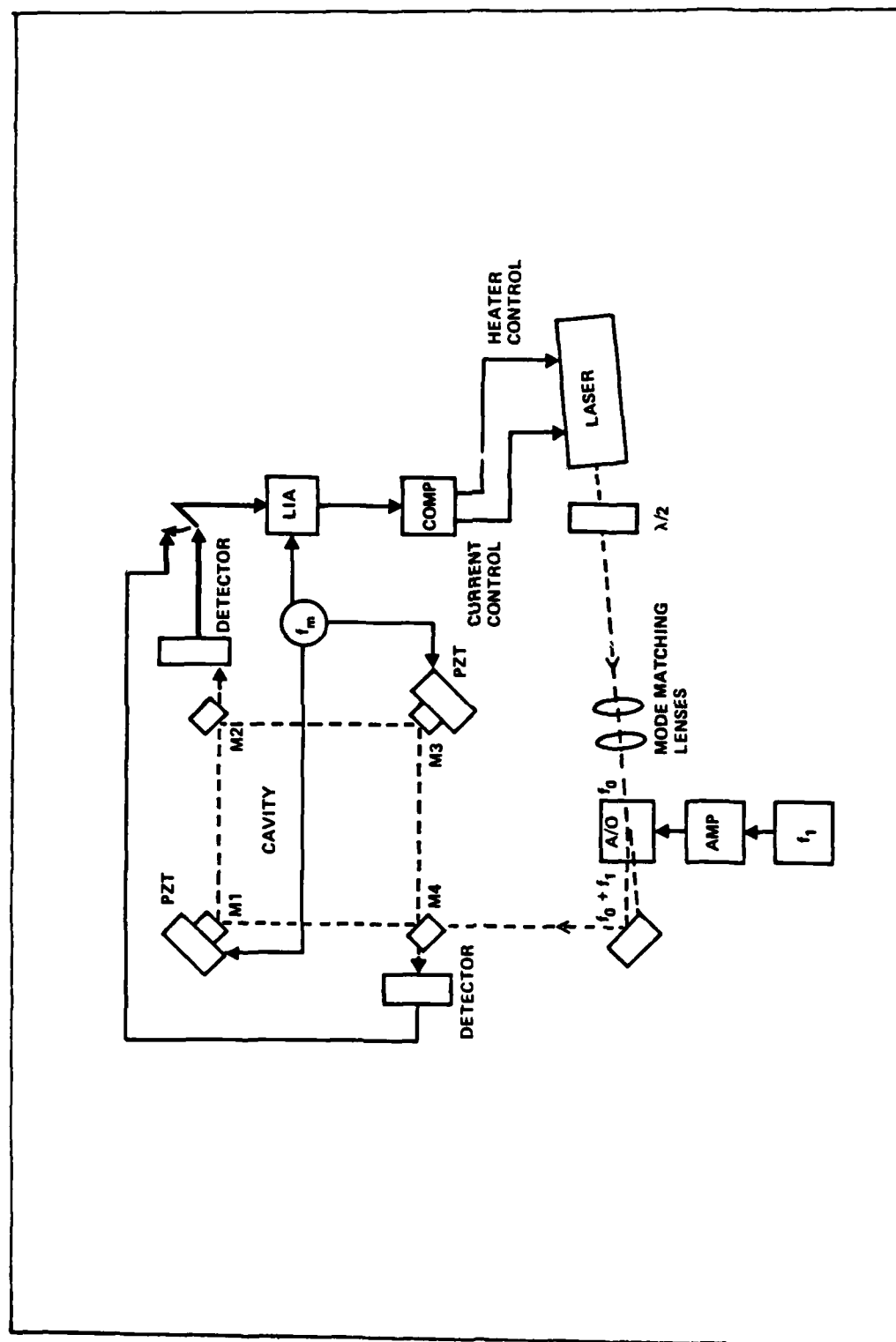
Fig. 3.3. Laser Stabilization Setup

Photodetectors and preamplifiers are positioned so that the beams transmitted through and reflected from the resonant cavity can be monitored. In this way, the laser's frequency can be locked to either the resonant peak of the transmitted beam or the resonant valley of the reflected beam. Appendix B presents the photodetector and preamplifier schematic. The output of one of the photodetector-preamplifier circuits is sent to a lock-in amplifier (LIA); the LIA generates an error signal to drive the compensation electronics which apply the correcting signals to the laser control electronics.

Modulation Signals. The feedback loop requires an error signal that indicates the laser frequency deviation from the cavity resonant frequency. The error signal is produced by introducing a 30 KHz modulation signal, $f_m$ in Figure 3.3, to the cavity PZTs to modulate the length, and hence, the resonant frequency of the cavity. The amplitude of the modulation signal is adjusted for maximum sensitivity of the error signal to cavity resonance. Figure 3.4 presents two examples showing how the error signal is produced by cavity modulation.

The first case shows the cavity resonant frequency being modulated about the resonant valley. The minimum voltage from the photodetector occurs when the modulation signal is zero voltage. At each minimum and maximum of

MODULATION
SIGNAL

DETECTOR
OUTPUT

0.5

DEMODULATED
SIGNAL

1.0

MODULATION
SIGNAL

LIA OUTPUT
(ZERO)          0

**MODULATION ABOUT RESONANT VALLEY**

MODULATION
SIGNAL          0

DETECTOR
OUTPUT          +

0.5

0

1.0

DEMODULATED     0
SIGNAL

MODULATION
SIGNAL

LIA             0
OUTPUT          –

**MODULATION ABOUT HALF POWER POINT**
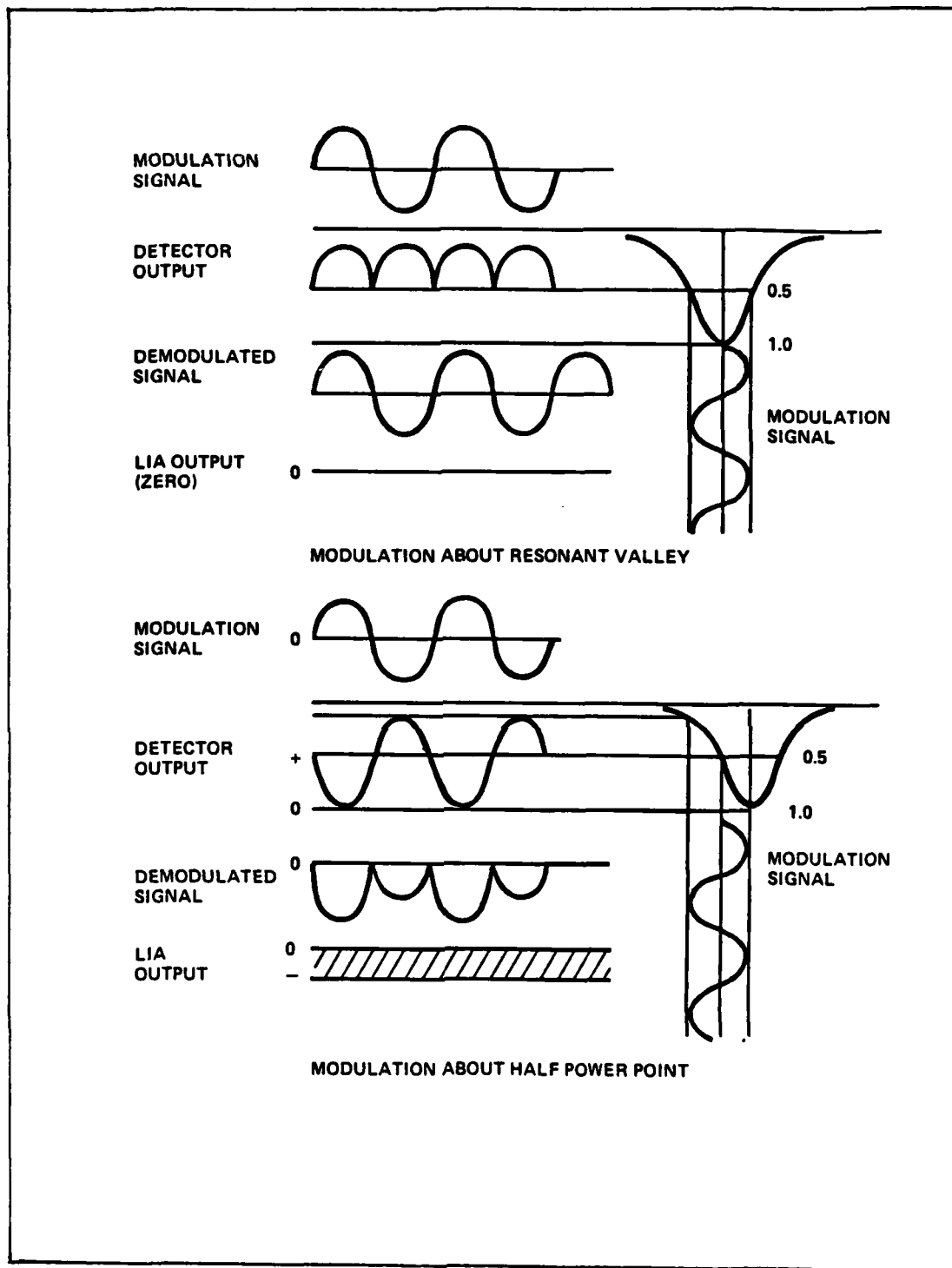
Fig. 3.4.   Resonant Valley Detection

47

the modulation signal the photodetector produces maximum

voltage. By sending both the modulation signal and the

photodetector signal into the LIA, a demodulated signal

is produced and subsequently integrated to give a DC error

signal. Since the resonant valley is symmetrical, the

demodulated signal is symmetrical about its axis. Mathe-

matical integration of this signal yields a zero DC error

signal.

As shown for the second case, the modulation sig-

nal is not centered on the resonant valley. The photo-

detector senses minimum power at the peak of the modula-

tion signal and senses maximum power at the minimum point

of the modulation signal. After combining the photo-

detector signal and the modulation signal in the LIA, the

resulting demodulated signal is no longer symmetric about

its axis. Therefore, a nonzero DC error signal is pro-

duced following the integration of the demodulated signal.

Controller Circuit. The compensation circuits

mentioned earlier receive the error signal enroute to the

laser frequency control electronics. The schematic dia-

gram for the compensator is shown in Figure 3.5. The com-

pensator is essentially a two-stage proportional plus

integral controller with adjustable gain and lead. The

first two op-amps amplify and integrate the incoming error

signal to produce the correcting signal for the current
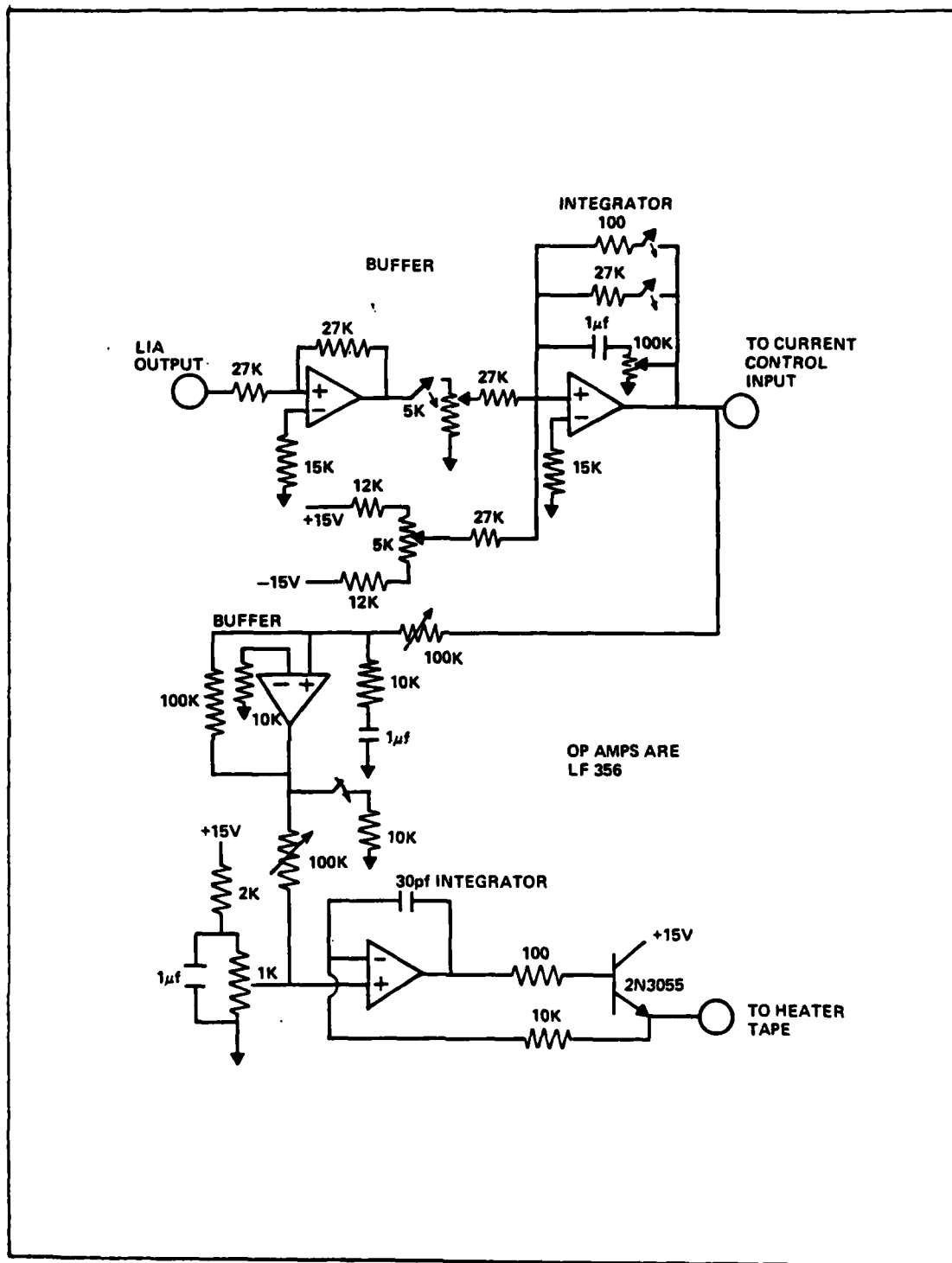
Fig. 3.5.   Laser Compensation Circuit

control. Because of the slower response of the heater, the signal is sent through a 10 Hz low-pass filter and integrated again. A power transistor controls the current through the heater coil.

As there was no existing model for the system under control, the choice of controller gains could not be determined a priori by classical or modern control techniques. Therefore, the gains had to be determined experimentally, using "observed stability" and "perturbation response" as criteria. After numerous iterations a combination of gains that yielded a stable response was found.

The proportional and integral gains were subsequently tuned slightly to improve stability and response time to input perturbations. Perturbation signals were sinusoidal and summed with the PZT modulation signal. The tuning was accomplished by observing the frequency spectrum of the error signal on a Fourier analyzer. Ideally, only a frequency component at twice the modulation frequency should have been detected. Gains that minimized other frequency components while maximizing the $2f_m$ component were selected.

## PRRLG

After ensuring proper operation of the laser frequency stabilization loop, the setup was modified to operate as a PRRLG as shown in Figure 3.6. Following
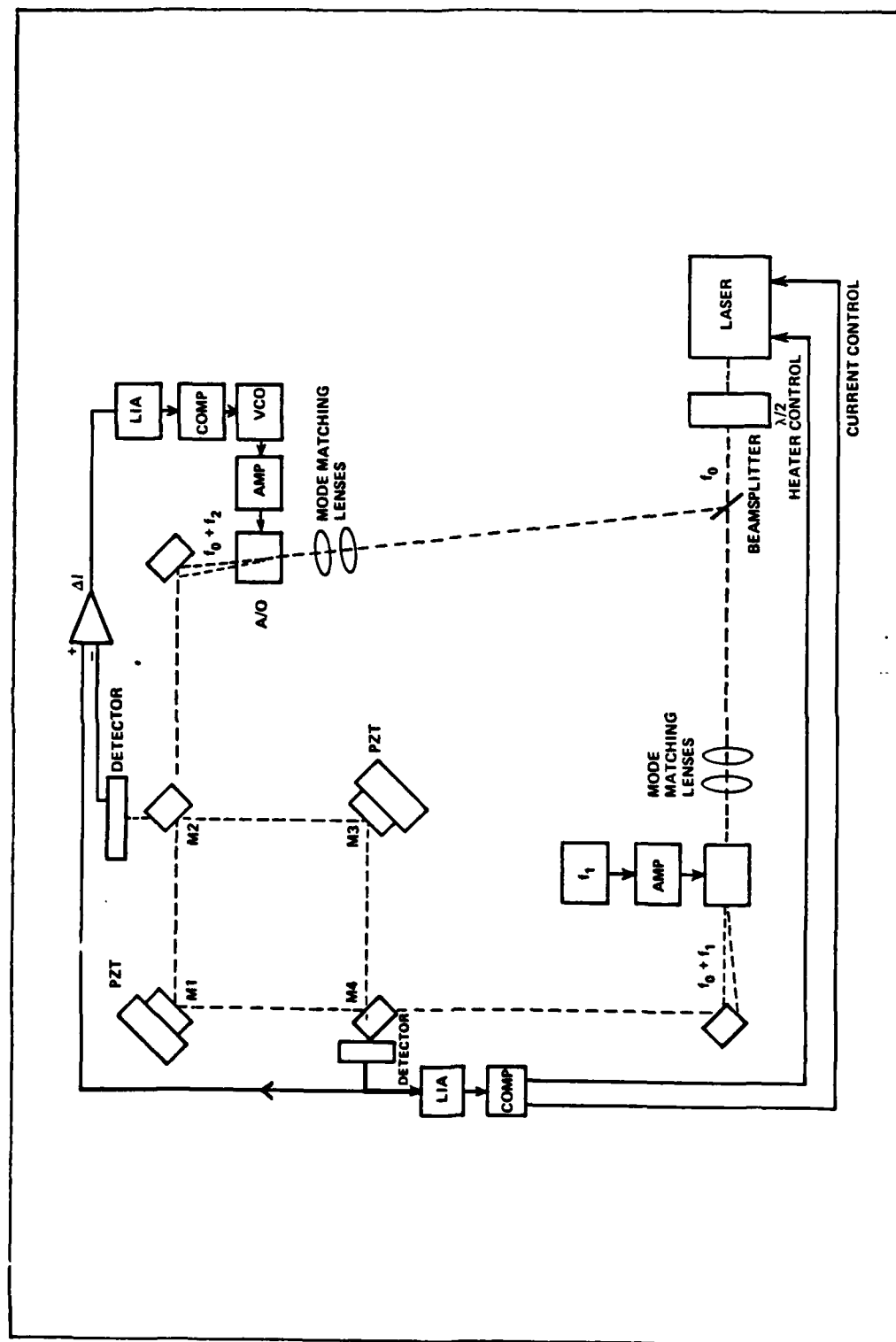
Fig. 3.6. PRRLG Setup

previous designs (5; 9; 12; 15; 18; 22; 26), a secondary feedback loop was added, which adjusted the frequency, $f_2$, of the voltage controlled oscillator (VCO) driving the A/O in the clockwise beam path so that $f_0 + f_2$ matched the clockwise resonant frequency of the cavity. The signals for this loop originate at the outputs of the two photodetectors which monitor the reflected intensity from the two input mirrors. The signals corresponding to the two intensities are differenced at the LIA to reduce residual noise common to both beams. In the same manner as the laser stabilization loop, this signal is demodulated and integrated by the LIA. The output of the LIA is then compensated by a proportional plus integral controller whose output is then used to drive a VCO to produce $f_2$. Figure 3.7 shows the compensation circuit for this loop. As before, the gains for the controller were determined experimentally using "observed stability" and "perturbation response."

## Assembly

To avoid excitation of higher-order transverse modes in the cavity due to beam misalignment, stable optical mounts and an accurate mode matching design were used. All experiments were conducted in a temperature controlled environment, and the optical elements were fastened to a thermally stable Invar base. To reduce vibration effects,

52
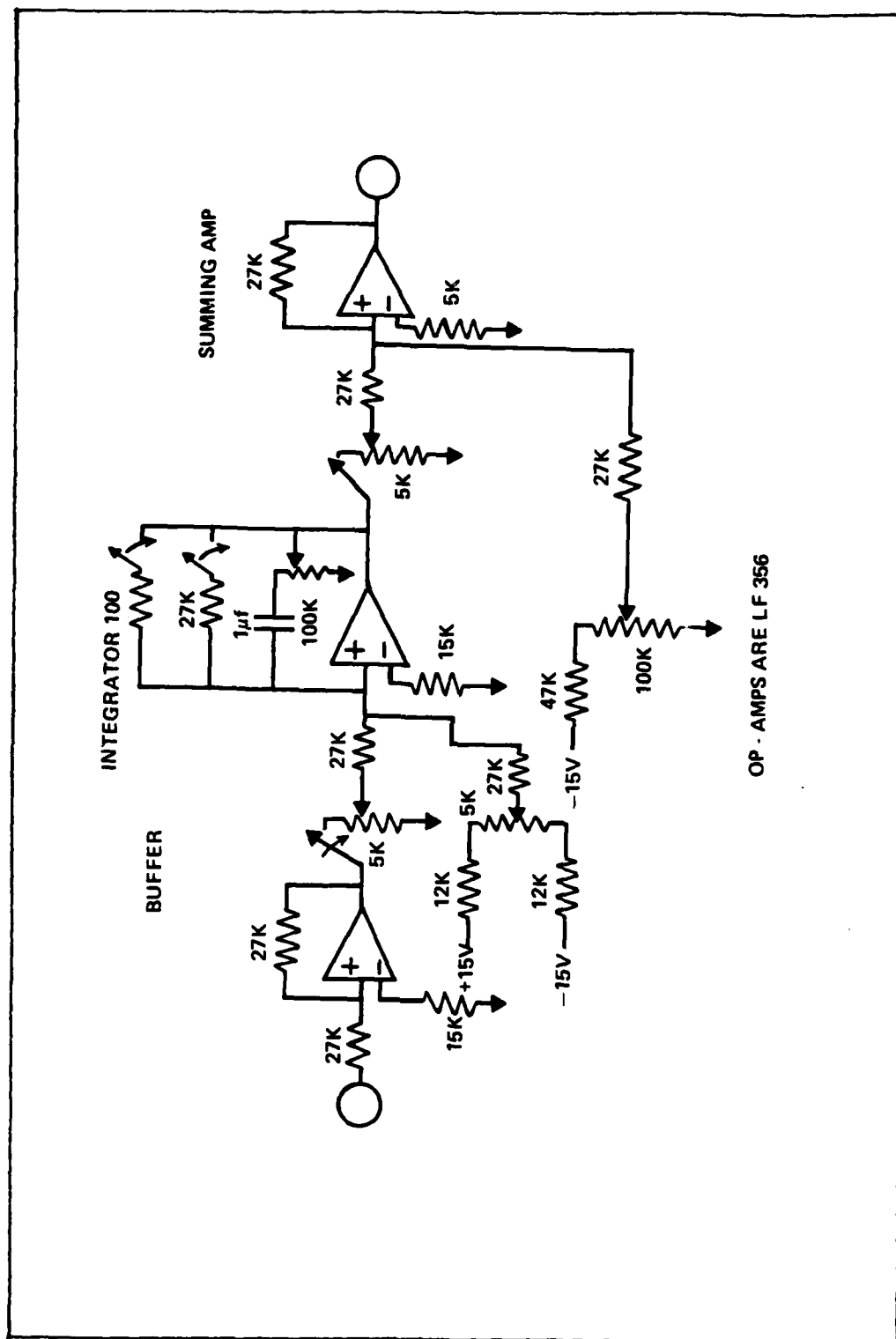
Fig. 3.7. Secondary Loop Compensation Circuit

the Invar base was mounted on a rate table mounted atop one of the isolation piers of the "seismically stable plat- form" in the Seiler Laboratory. To reduce high frequency vibration further, foam padding was placed between the Invar base and the rate table.

The electrical components were mounted on a rack external to the test table. Connections from the elec- trical components to the optical components were made by coaxial cables strung from the test rack through overhead hangers to the test table. The test table slip rings were not used since they transmit noisy high frequency signals. Figures 3.8 and 3.9 show far and close-up views of the assembly.

## Alignment

The alignment of the laser beam and the cavity is a crucial step in the construction of the PRRLG. First, the laser beam must be leveled with respect to the base. Next, the A/O position is adjusted so that the intensity of the first-order beam is maximized. With the proper combination of positioning the laser, the corner mirror and the cavity, the first-order beam can be aligned with the cavity. The result is a visible beam being transmitted through the cavity when a 10 Hz, 20 volt peak-to-peak sig- nal is applied to the cavity PZTs. This signal is required because the uncontrolled laser frequency is not at the

54
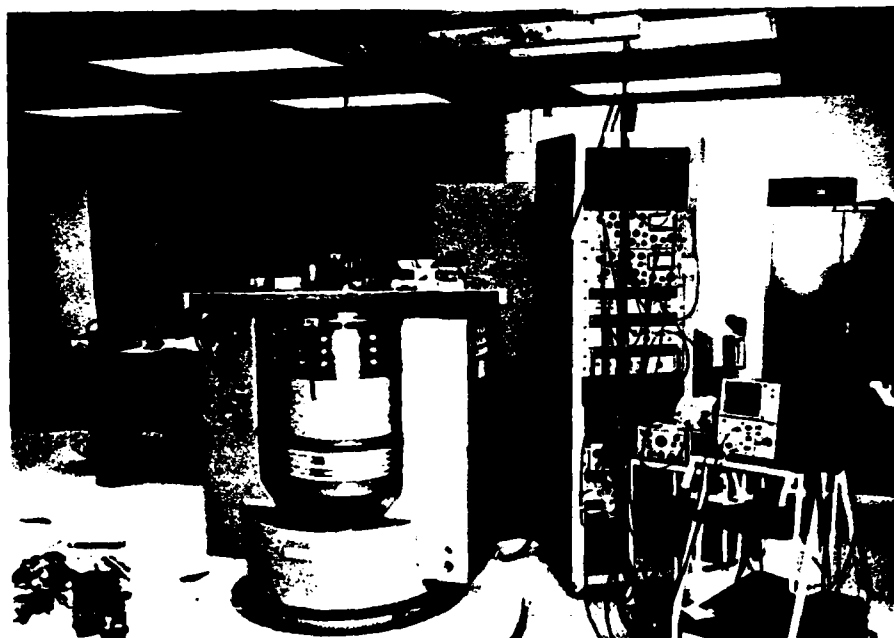
Fig. 3.8.   PRRLG and Associated Equipment
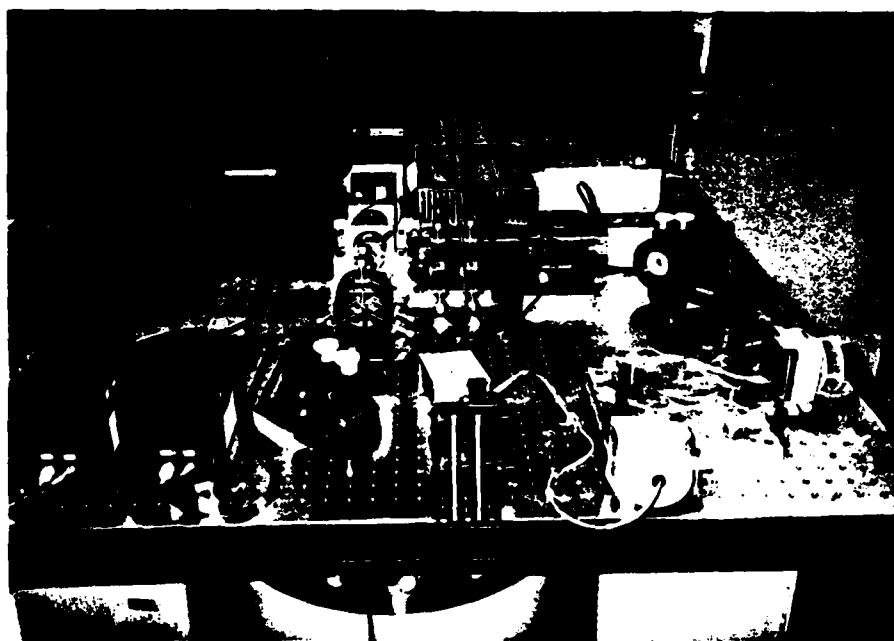


Fig. 3.9.   PRRLG Components Mounted on Invar Table

resonant frequency of the cavity. By varying the optical path length of the cavity, the cavity resonant frequency can be made to coincide with the laser frequency at some point during the modulation cycle.

Once a beam is transmitted, an oscilloscope is connected to the output of the detector to monitor the transmitted intensity. By changing the beam's angle of incidence to the corner mirror and by translating the beam using refraction through a thick glass plate, the $TEM_{0,0}$ mode can be maximized and higher-order TEM modes can be minimized. This process is completed for both of the beams being injected into the cavity. Figure 3.10 shows the oscilloscope trace of the monitored transmitted intensity (mode matching lenses not inserted yet). The large peaks corresponds to the intensity of the $TEM_{0,0}$ mode being trans-mitted through the cavity. The smaller peaks corresponds to the transmission of higher-order modes.

TRANSMITTED
INTENSITY
500 mV/div

SCAN
VOLTAGE
20 V/div
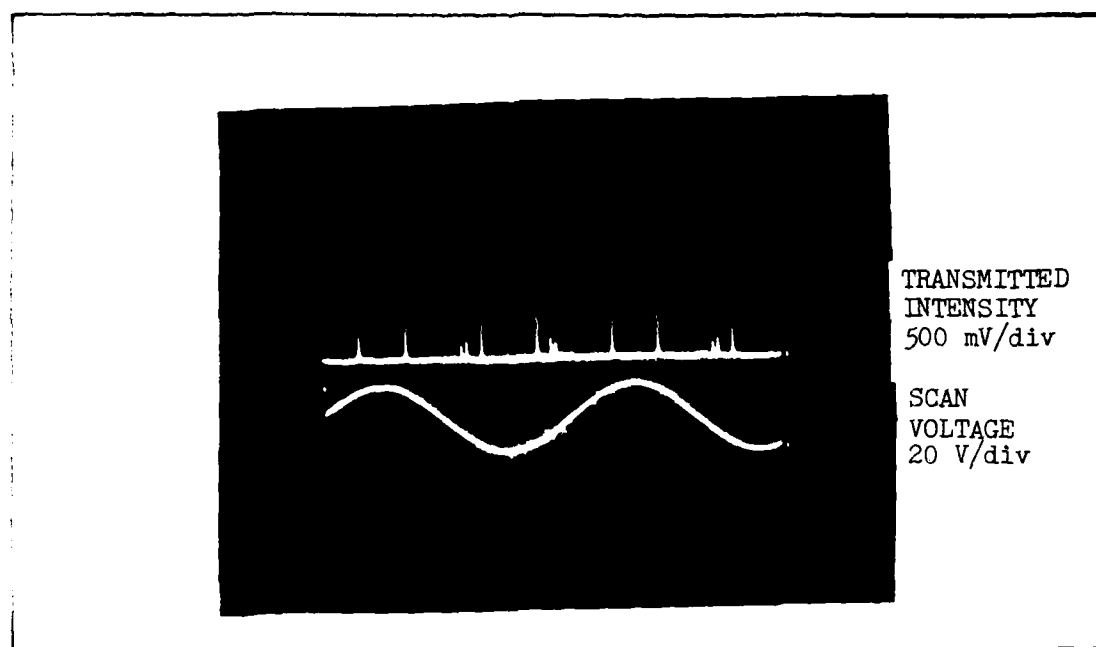
Fig. 3.10.   Transmitted Beam Intensity

# IV.  Results

The data taken falls into two general categories: preliminary data and performance data.  The preliminary data includes measurements of beam intensity, cavity free spectral range, linewidth and finesse.  The performance data includes measurements of PRRLG bias, bias drift, and random error.

## Preliminary Data

Beam Intensities.  So that the beam intensities in both directions can be balanced, intensity measurements are taken at three locations for each beam.  The first measurement is taken just before the two beams enter the cavity.  The second measurement compares the reflected beam intensities and the third compares the transmitted beam intensities while the laser is locked to the cavity. The intensities were equalized by varying the amplitude of the acoustic wave in the A/O as described in Chapter II. Table 4.1 shows the beam intensities at the three locations before and after adjusting the A/O.  Although the intensities in each of the three cases varied from test to test, the clockwise and counter-clockwise intensities were equalized to this degree prior to the start of any test.

TABLE 4.1

BEAM INTENSITIES

|  | Intensity Before A/O Adjustment ($\mu$ watts) | | Intensity After A/O Adjustment ($\mu$ watts) | |
|---|---|---|---|---|
|  | CW | CCW | CW | CCW |
| Before Entering Cavity | 205 | 222 | 215 | 216 |
| Cavity Transmission | 88 | 94 | 90 | 90 |
| Cavity Reflection | 101 | 113 | 105 | 105 |

Free Spectral Range. The free spectral range of the cavity is 576.92 MHz as calculated by Equation (2.17). We relate the PZT voltage to frequency by determining the voltage that causes a 576.92 MHz shift in the cavity resonant frequency. This is accomplished by applying a saw-tooth scan voltage to the cavity PZTs and monitoring the transmitted intensity with the photodetector (control loops are open). If both the scan voltage and the intensity voltage are displayed simultaneously, the difference in scan voltage between two adjacent resonant peaks can be determined. This voltage difference is proportional to the cavity free spectral range and the resonant frequency shift per volt can be determined. Figure 4.1 shows the strip chart displaying both the scan voltage and the transmitted intensity. As shown in the figure, the voltage required to drive the cavity resonant frequency across

59
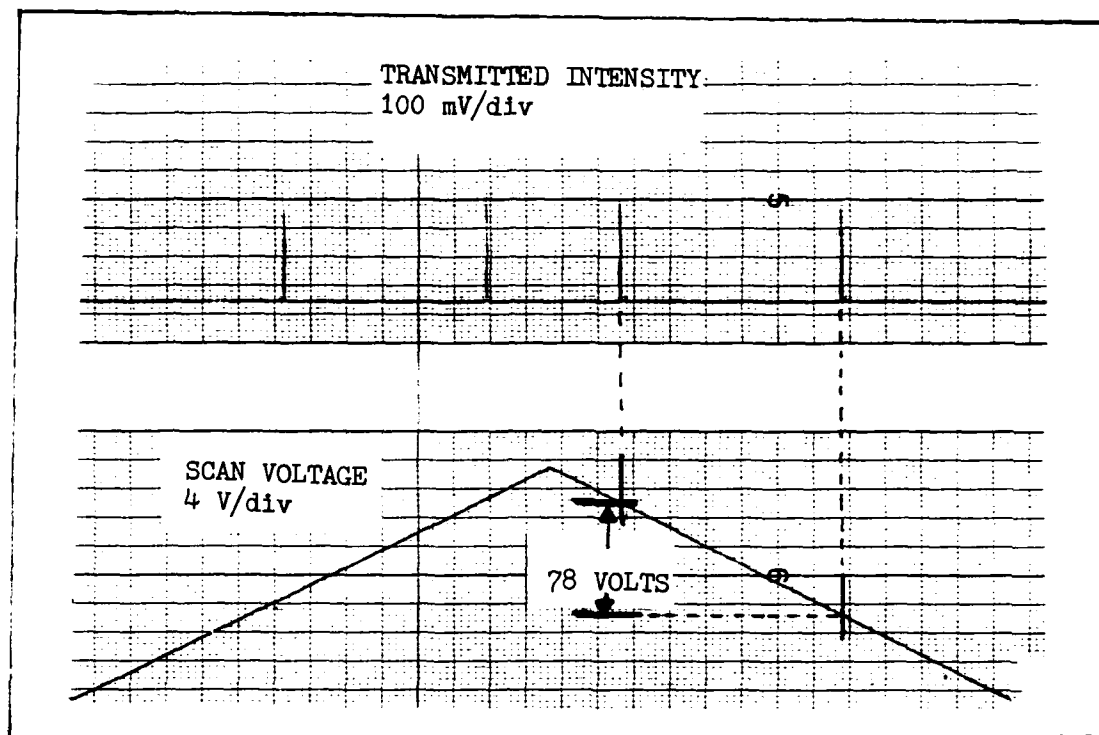
Fig. 4.1.  Cavity Free Spectral Range

a full free spectral range is 78 volts, which translates
to a frequency shift of 7.396 MHz/volt.  From this, the
cavity linewidth and finesse were found using a new method
described below.

Cavity Linewidth and Finesse.  Because the frequency
drift in the uncontrolled laser was so high (> 1 MHz/sec),
determining the cavity linewidth in the traditional manner
(14:IV-2) was abandoned.  Instead, a new method was devel-
oped which required a commercially frequency stabilized
He-Ne laser.  This laser was set up so that the beam was
divided by the beamsplitter and traveled along the

counter-clockwise beam path of the original laser. The
new laser was aligned with the cavity so a transmitted
beam could be observed. The PZT bias was adjusted until
the resonant peak of the transmitted beam was located and
then a low amplitude, 100 Hz modulation signal was applied
to the PZTs. The amplitude of the modulation signal was
adjusted until the PZTs modulated the cavity about the
half-power points of the resonant peak. The voltage
required to do this then corresponded to the cavity line-
width.

Figure 4.2 displays the scope trace used to deter-
mine the cavity linewidth. The top trace is the reflected
intensity, the middle trace is the modulation signal and
the bottom trace is the transmitted intensity. As shown,
the modulation signal of 3 millivolts was required to change
the resonant frequency of the cavity by the cavity line-
width (transmitted intensity drops from 1.5 to .75 volts
during the modulation cycle). This corresponds to a line-
width ($\Gamma$) of 22.2 KHz. Since the cavity finesse (F) is
defined by

$$F = FSR/\Gamma$$

then the cavity finesse is computed to be 25987. The com-
puted values for cavity linewidth and finesse differ from
those estimated earlier in Chapter III because Equations
(2.18) and (2.19) used in estimating finesse assume a loss-
less cavity.

61

REFLECTED
INTENSITY
500mV/div

SCAN
VOLTAGE
5 mV/div

TRANSMITTED
INTENSITY
1 V/div

.005 msec/div
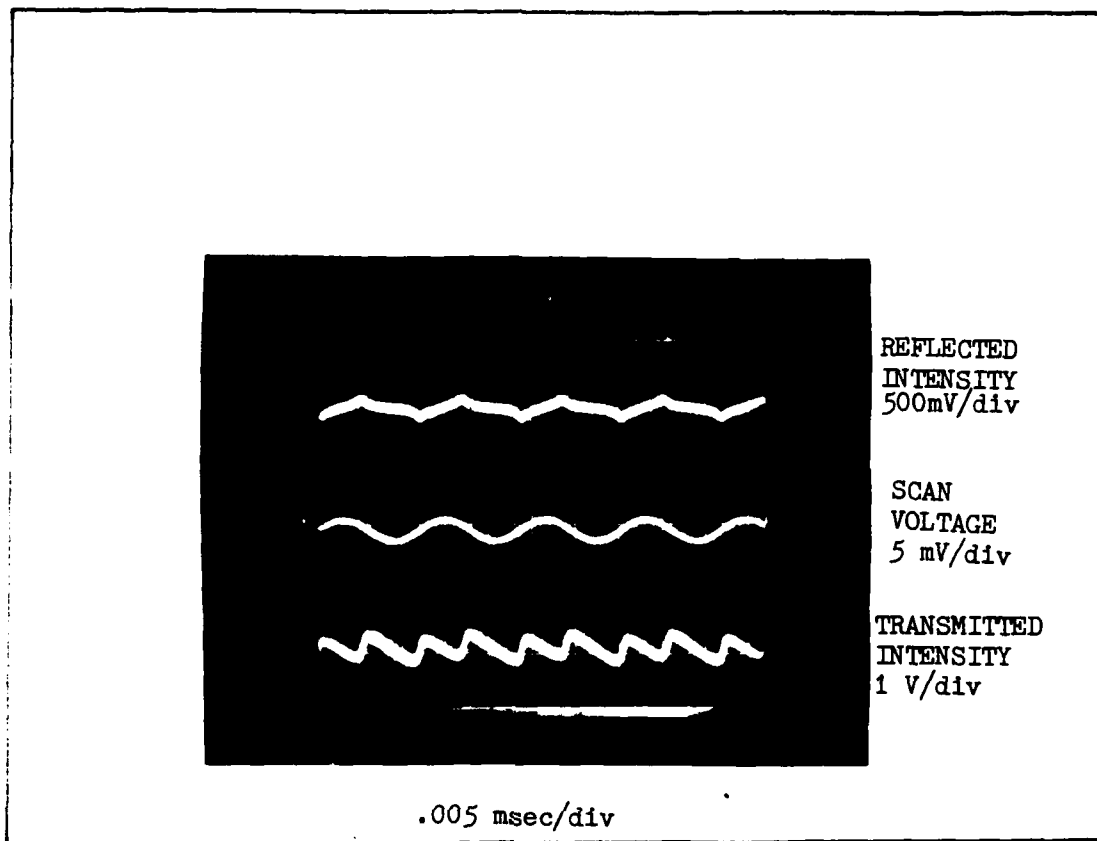
Fig. 4.2.  Cavity Linewidth Measurement

## Performance Data

As described earlier, in the presence of an
inertial rotation rate normal to the plane of the PRRLG,
the frequency of the two resonant beams differ in accord-
ance with the Sagnac effect as given by Equation (2.39).
Assuming perfect operation of the control loops, the pri-
mary error source in PRRLGs (11:479) is the inability to
achieve the precise frequency required to resonate at the
peak of the transmitted intensity curve (or the valley of

62

the cavity reflected intensity curve) which maps into an uncertainty $\delta\Omega$ in determining the rotation rate $\Omega$. The fundamental shot-noise limit in determining $\Omega$ is (11:479):

$$\delta\Omega = \frac{\lambda P}{4A} \frac{\sqrt{2}\ \Gamma}{(N\eta\tau)^{\frac{1}{2}}} \tag{4.1}$$

where

> $P$ = the perimeter of the ring (m)
>
> $A$ = the area enclosed by the resonant ring in (m$^2$)
>
> $\lambda$ = the wavelength of the laser light in (m)
>
> $\Gamma$ = the cavity linewidth (Hz)
>
> $N$ = the number of photons striking the detector per sec
>
> $\eta$ = the detector efficiency
>
> $\tau$ = the averaging time (sec)
>
> $\delta\Omega$ = uncertainty in determining the true rotation rate (rad/sec)

The PRRLG was subjected to the vertical component of earth rate while a frequency counter measured the difference frequency $f_2 - f_1$ of the A/Os for one second sample times. The data was recorded directly onto a floppy disk for posttest processing. Appendix C contains detailed test procedures as well as the data reduction method.

Analysis of the experimental data from five separate tests showed an average rate bias of 0.99 Earth Rate Units (ERU) and an average long-term bias drift of 0.103 ERU/hr. Table 4.2 presents the bias and bias drift

TABLE 4.2

BIAS AND BIAS DRIFT RESULTS

| Test Number | Duration (seconds) | Bias (ERU) | Bias Drift (ERU/hr) |
|---|---|---|---|
| One | 16000 | 0.95 | 0.111 |
| Two | 15000 | 1.12 | 0.095 |
| Three | 15000 | 1.01 | 0.115 |
| Four | 15000 | 0.98 | 0.092 |
| Five | 16000 | 0.89 | 0.102 |
| Average | | 0.99 | 0.103 |
| Standard Deviation | | 0.085 | 0.0099 |

values for each test. These parameters show good test to test repeatability as the standard deviation of the bias and bias drift across the five tests was 0.085 ERU and 0.0099 ERU/hr, respectively.

For an averaging time of 1 second, the average random error (standard deviation of residuals) was 0.0259 ERU. Table 4.3 presents the random error measurements for each test for sampling times of 1, 10, 100 and 1000 seconds. The average random error as a function of averaging time is presented in Figure 4.3. The solid line represents the shot noise limitation of the PRRLG as a function of $\tau$.
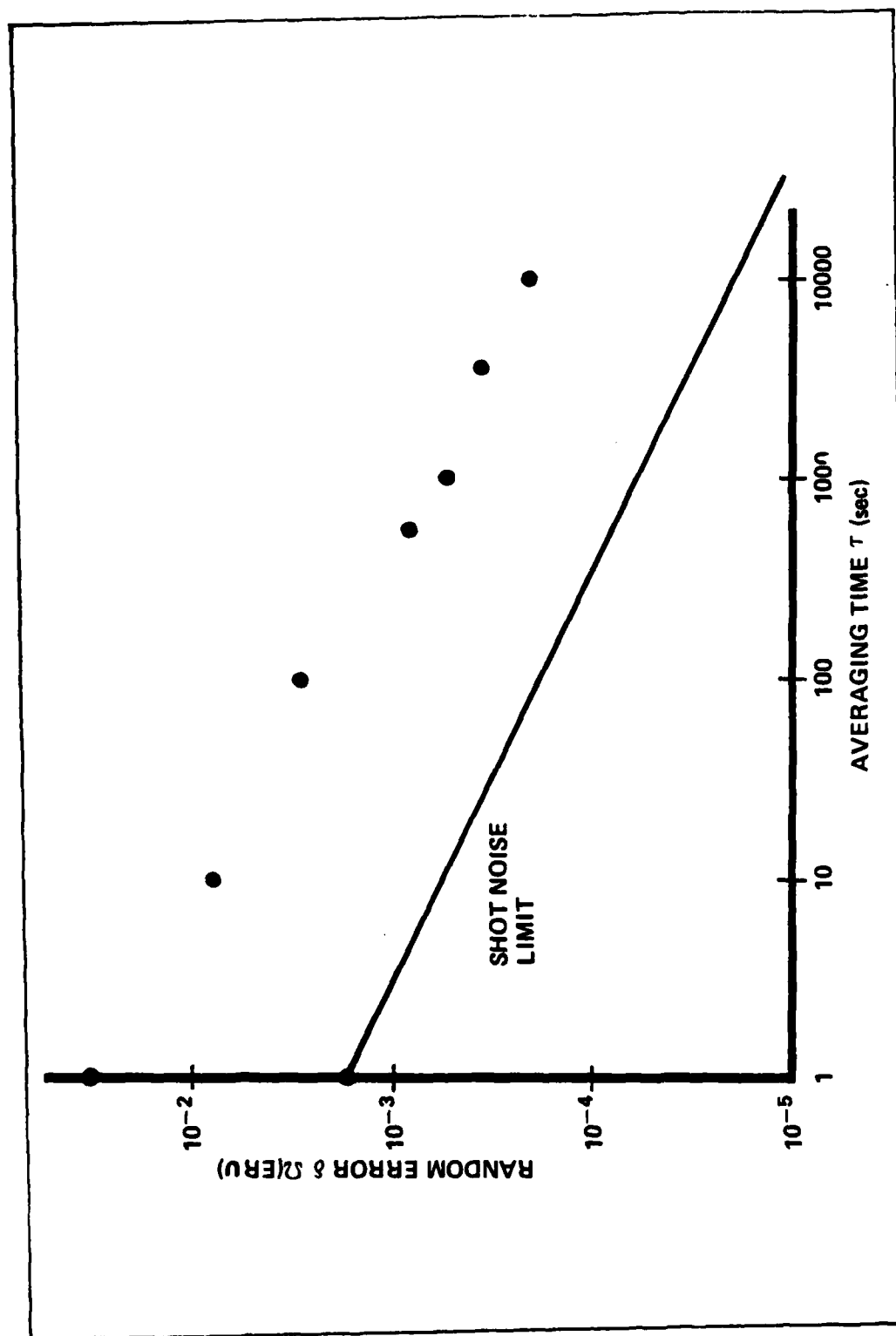
Fig. 4.3. Random Error versus Sampling Time

65

TABLE 4.3

RANDOM ERROR RESULTS

| Test | Random Error in ERU for Averaging Time | | | |
| | $\tau = 1$ sec | $\tau = 10$ sec | $\tau = 100$ sec | $\tau = 1000$ sec |
| --- | --- | --- | --- | --- |
| One | 0.0185 | 0.0066 | $2.52 \times 10^{-3}$ | $5.44 \times 10^{-4}$ |
| Two | 0.0392 | 0.0104 | $4.01 \times 10^{-3}$ | $7.68 \times 10^{-4}$ |
| Three | 0.0177 | 0.0063 | $2.69 \times 10^{-3}$ | $5.27 \times 10^{-4}$ |
| Four | 0.0244 | 0.0072 | $2.61 \times 10^{-3}$ | $6.62 \times 10^{-4}$ |
| Five | 0.0297 | 0.0085 | $2.98 \times 10^{-3}$ | $5.96 \times 10^{-4}$ |
| Average | 0.0259 | 0.0078 | $2.96 \times 10^{-3}$ | $6.19 \times 10^{-4}$ |
| SD | 0.0089 | 0.0017 | $6.11 \times 10^{-4}$ | $9.83 \times 10^{-5}$ |

Error Sources. The primary cause for the long-term bias drift was found to be linked to a drift in the signal corresponding to the difference between the two reflected intensities used to drive the A/O loop. Although the reflected intensities were equal prior to the test, the intensity difference, $\Delta I$, drifted during the tests. The bias drift, highly correlated to the $\Delta I$ drift, then resulted. Figure 4.4 shows a plot of the beam intensity difference versus the measured rotation rate as given by the difference frequency between the counterrotating beams.

Perhaps the predominant reason that the performance of the PRRLG was not at the shot-noise limit was because the linewidth of the laser was not narrowed enough by the
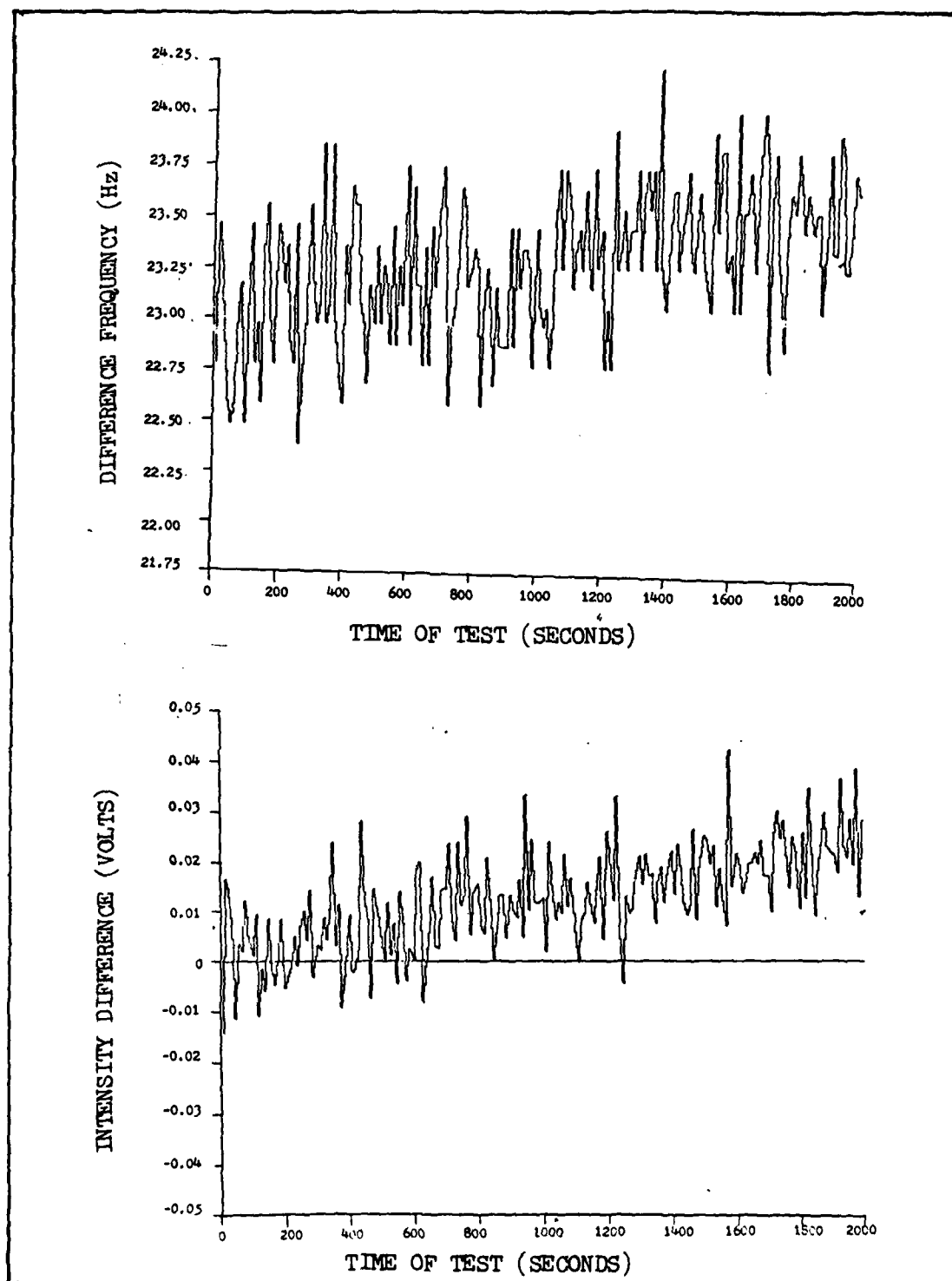
Fig. 4.4.  Bias Drift and Beam Intensity Difference

67

frequency stabilization loop. The measurements taken of reflected and transmitted intensity while in resonance indicate that a portion of the laser energy was outside the bandpass of the cavity. Since the cavity could not pass that frequency of light, it was reflected by the cavity into the photodetector and degraded the signal-to-noise ratio. Appendix D presents other observations relating to the laser frequency stabilization.

Another cause for performance not at the shot noise limit could be inaccurate mode matching. If this occurred, then all of the laser energy would not be transferred to the cavity; a portion would be reflected into the photodetector, thereby increasing the signal-to-noise ratio. Appendix D presents other observations relating to the laser frequency stabilization.

Unfortunately, in achieving a thermally stable environment, air currents and pressure changes caused by the environmental control unit were encountered. This induced a considerable amount of phase noise in the reflected beam and led to an increase in noise in the detector output. In addition, the pressure changes due to air currents caused beam misalignment and excitation of higher-order transverse modes. Because the noise was outside the bandwidth of the controller, the electronics could not compensate for it.

Backscattering from the optical elements was also a source of error. The scattering caused low frequency noise to corrupt the intensity measurements, thus giving an uncertainty in maintaining resonance with the cavity. Backscattering also caused the formation of auxiliary interferometers between the optical elements, which directed energy back into the laser. This caused the lock-in phenomena as seen in active RLGs but on a significantly smaller scale.

# V.   Conclusions and Recommendations

The results from this experiment are encouraging for the development of the 58 $m^2$ PRRLG.   Comparing the performance of this PRRLG to one constructed by Nelson (12) shows an improvement in both random error (0.0078 ERU vs 0.018 ERU) and bias drift (0.103 ERU/Hr vs 2 ERU/Hr). In this experiment, Nelson used the PZTs to lock the resonant frequency of a 9000 finesse cavity to the frequency of a commercially stabilized laser.   The finesse here is 25,000 and the electrical components used are the same as Nelson used.

With several modifications and improvements, this new approach will be feasible for extrapolation to the larger ring.   For example, the long-term bias drift could be diminished by real-time control of the amplitude of the acoustic wave in the A/O.   By controlling the amplitude of the signal driving the A/O, the amplitude of the frequency-shifted beam could also be controlled.   Using the equipment currently available at the Seiler Lab, the only way to control the amplitude of the signal driving the A/O is to use a microcomputer to sample the counterrotating beam intensities, and based on some logic, command the frequency synthesizer to alter the amplitude of its output.

Because the rate of change of the intensity difference is relatively slow compared to a potential sample rate of the microcomputer, this proposal would have sufficient bandwidth to eliminate the bias drift.

To improve the low signal to noise ratio observed in the reflected beam, a more efficient laser frequency stabilization method is required. One possibility would be to use the setup shown in Figure 5.1 to monitor both the reflected and transmitted beams of both counterrotating beams. The combination of Faraday isolators and polarizers allow the steering of the transmitted beam into the photo-detector while the oppositely directed beam is injected into the cavity. Using this configuration, information derived from the stable, more accurate transmitted beam could be used to drive a slow control loop and the high bandwidth obtained from the quick, but noisy, reflected beam could drive a fast control loop.

Another possibility for improvement of the frequency stabilizer was recently demonstrated at the Joint Institute of Laboratory Astrophysics in Boulder, Colorado. This work developed a laser stabilization technique which yielded a sub-Hz laser linewidth (10). Incorporation of the new controller circuit into the PRRLG should improve performance significantly.

Dr. Ezekiel (18) demonstrated that putting a phase modulator in either beam before injection into the cavity
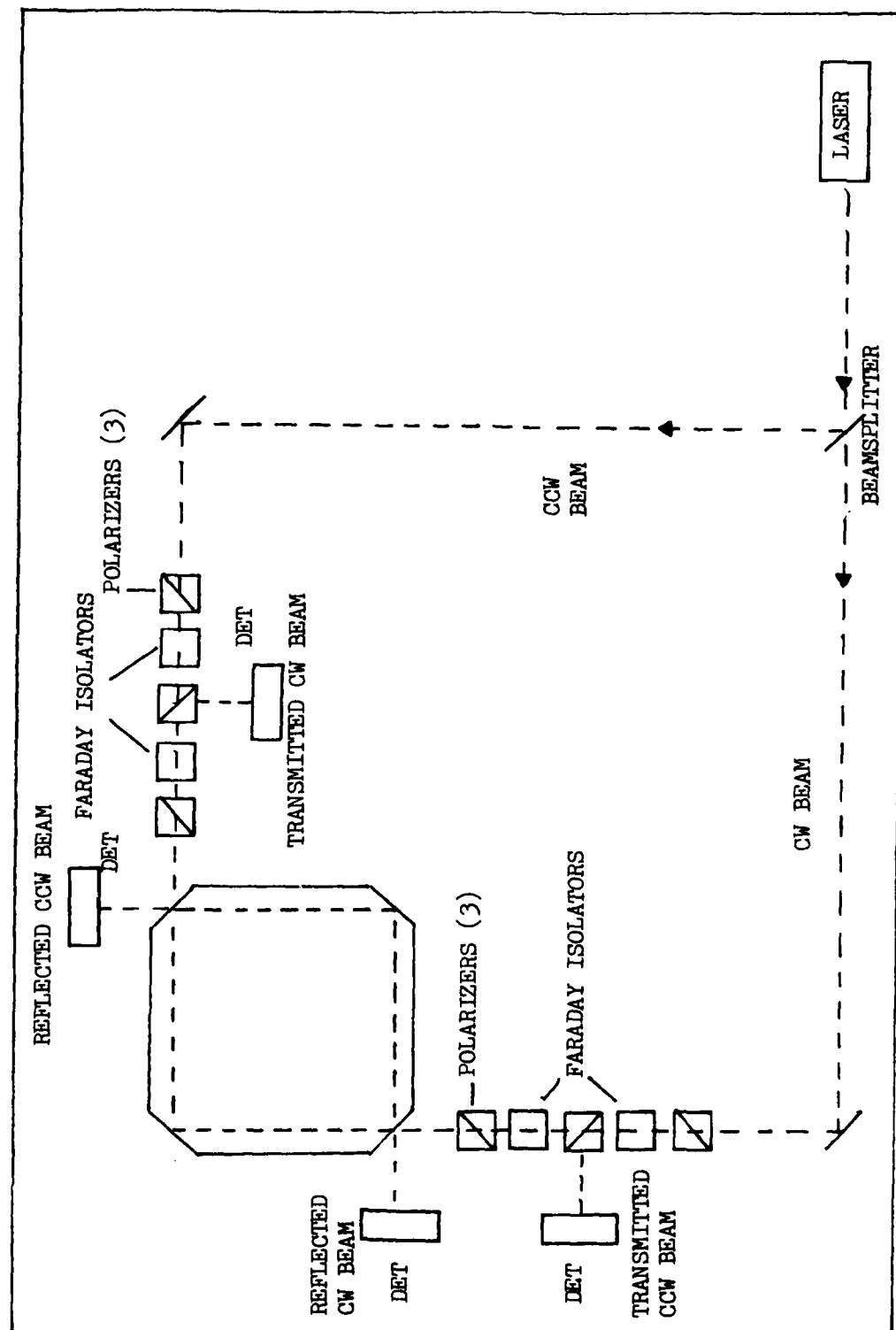
Fig. 5.1. . Monitoring of Transmitted and Reflected Intensity

reduces scattering. The use of this phase modulator as a dither instead of the PZTs would allow increased closed loop bandwidth. Phase noise due to pressure changes and air currents could be alleviated by isolating the PRRLG assembly with a plexiglass cover. One has already been designed and constructed at the Seiler Lab, which is useable only with modification of the component placement.

Finally, results indicate that the extrapolated performance of the 58 $m^2$ PRRLG can reach the geokinetic and relativity experimental accuracies. Assuming nominal values for the variables in Equation (4.2) of

$$N = 3.2 \times 10^{18}$$

$$n = .5$$

$$\tau = 10 \text{ seconds}$$

$$\Gamma = 250 \text{ Hz}$$

$$A = 58 \text{ m}^2$$

$$P = 30.46 \text{ m}$$

the shot-noise limit for the 58 $m^2$ PRRLG would be $1 \times 10^{-10}$ ERU. If the actual performance were an order of magnitude higher, the projected random error would be about $10^{-8}$ to $10^{-9}$ ERU. Note, however, that the above-mentioned improvements may improve performance of the 58 $m^2$ PRRLG to closely follow the shot noise limit, thus giving the desired sensitivities for the geophysical and relativity experiments.

# Appendix A: Mode Matching

In a passive RLG, the laser cavity and resonant cavity are separate and, therefore, each cavity has its own characteristic mode. To allow for the maximum transfer of power from the laser into the resonant cavity mode, the laser mode must be shaped to coincide with the cavity mode. This is known as mode matching.

If mode matching is not accomplished, the laser beam directed into the cavity is not stable, and changes with each round trip until the beam degenerates into one or more of the cavity modes. The overall effect is a loss of power transmitted through the cavity and a decrease in the effective cavity finesse.

The mode matching procedure consists of: (1) characterizing the output of the laser by determining the size and location of the waist of the laser beam, (2) characterizing the mode of the cavity by determining the size and location of the waist of an imaginary beam resonating within the cavity, (3) finding locations along the beam path where the horizontal and vertical modes of the laser and the cavity match, and (4) inserting a cylindrical lens at each of these two points to cause the radius of curvature of the laser beam to match that of the cavity.

The size and location of the beam waist of the laser is determined using the setup shown in Figure A.1. Intensity measurements are taken at various positions of the knife edge. Using this data, a least square fit to the Gaussian beam intensity profile is made to find the spot size at that location from the laser output. This set of measurements is then repeated for several more
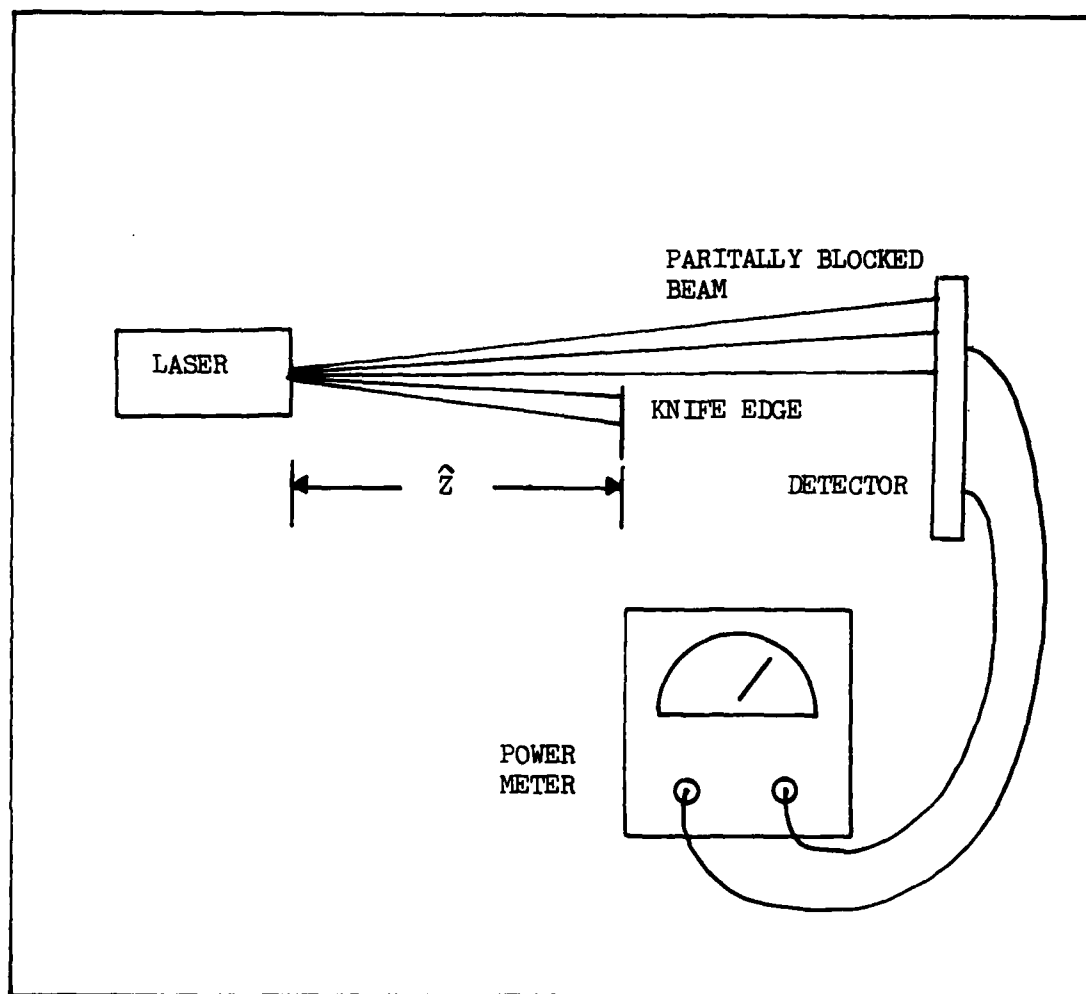


Fig. A.1.  Setup for Spot Size Measurements

TABLE A.1

SPOT SIZE MEASUREMENTS

| Distance from Laser Output $\hat{z}$ (cm) | Spot Size $\omega$ (cm) |
|---|---|
| 17.78 . . . . . . . . . . . . . . . . . . . . . | 0.0406 |
| 30.48 . . . . . . . . . . . . . . . . . . . . . | 0.0445 |
| 38.10 . . . . . . . . . . . . . . . . . . . . . | 0.0475 |
| 45.72 . . . . . . . . . . . . . . . . . . . . . | 0.0523 |
| 50.80 . . . . . . . . . . . . . . . . . . . . . | 0.0528 |

locations. Table A.1 shows the measured spot sizes at
several distances from the output of the laser. Using this
data, a least squares fit is made to

$$\omega(z)^2 = \omega_o^2 + (\frac{\lambda}{\pi\omega_o})^2 \hat{z} \qquad (A.1)$$

where

$\omega(z)$ is the spot size at a distance z from the beam
waist

$\omega_o$ is the spot size at the beam waist

$\lambda$ is the wavelength of the light

$\hat{z}$ is the distance from the beam waist

In this form, (z) versus z plots as a straight line with
$\omega^2(z)$ being the y-axis intercept and $(\frac{\lambda}{\pi\omega_o})^2$ being the slope
of the line.

The least-squares fit gives two different estimates of $\omega_0$ since the actual value of $\hat{z}$ is unknown. Using an iterative approach, an estimate for the bias in $\hat{z}$ is made. When the two values for $\omega$ are equal, the corresponding value for z is correct ($z = \hat{z}$ + bias). The result of this procedure provides the relative location of the beam waist with respect to the output of the beam and the spot size, $\omega_0$, at the beam waist.

Table A.2 shows the result of this least squares fit. The estimate in the bias in $\hat{z}$ implies that the beam waist is inside the laser cavity itself. This is reasonable as the two mirrors used to form the laser cavity are both spherical and, thus, form a confocal cavity.

The characteristic Gaussian mode of a cavity can be found by determining the unique Gaussian beam that "fits" the geometry of the cavity and the curvature of the cavity mirrors. First, consider the plano-spherical Fabry-Perot cavity as shown in Figure A.2. This cavity consists

TABLE A.2

BEAM WAIST LOCATION AND SIZE

| | |
|---|---|
| Bias in $\hat{z}$ . . . . . . . . . . . . . . . . . . . | −18.84 cm |
| Spot Size at Waist . . . . . . . . . . . . . . | 0.0341 cm |
| Correlation of Points . . . . . . . . . . . . . | .988 |

77
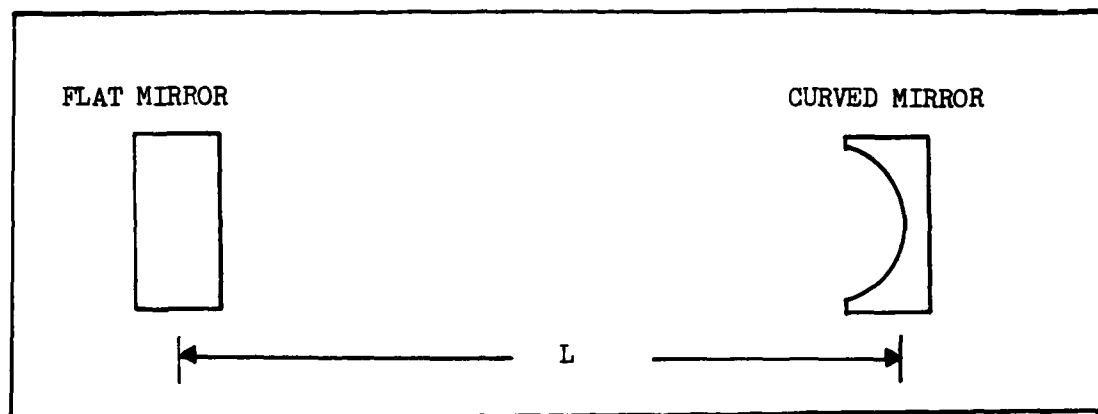
Fig. A.2.   Plano-Spherical Cavity

of a flat mirror, with an infinite radius of curvature,
and a spherical mirror, with a radius of curvature of R,
separated by a distance L from the flat mirror.  To "fit"
the flat mirror, the Gaussian mode must have a waist at
the flat mirror, since the radius of curvature at the beam
waist is infinite.  The beam's radius of curvature at L
must also match the radius of curvature, R, of the curved
mirror.  Manipulation of Equation (2.22) gives the size of
the beam waist as:

$$\omega_o = [\frac{\lambda}{\pi}(zR(z))^{\frac{1}{2}}(1-\frac{z}{R(z)})^{\frac{1}{2}}]^{\frac{1}{2}} \qquad (A.2)$$

These concepts can be extended to the symmetrical square
cavity of Figure A.3.  This cavity consists of two opposing
flat mirrors and two opposing spherical mirrors of equal
radius of curvature, R.  As before, the characteristic
Gaussian beam "fits" the radius of curvature of each

78
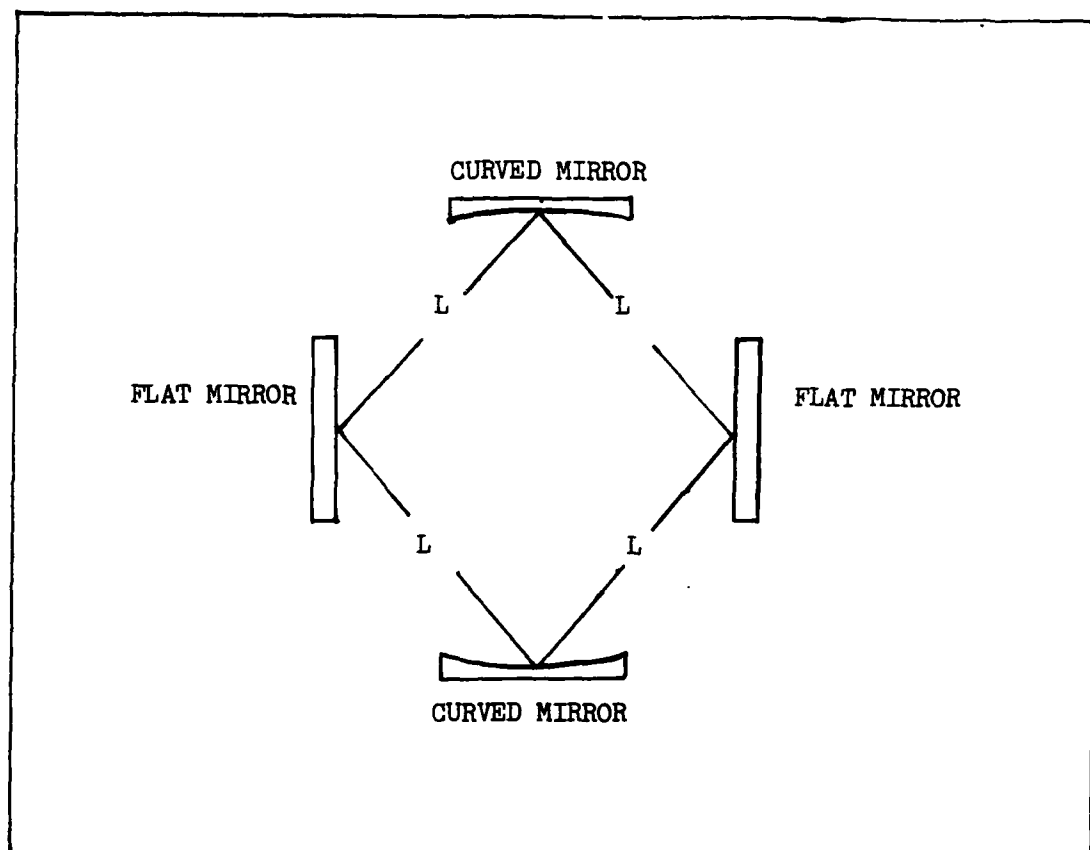
Figure A.3. Plano-Spherical Square Cavity

mirror. The square cavity will, therefore, have two
waists, one at each flat mirror.

Due to the 45 degree angle of incidence to the
spherical mirrors, a modification to the procedure must
be made. The 45 degree angle of incidence at the spherical
mirrors changes the effective radius of curvature of the
mirror. Because of this, the beam that "fits" R in the
square cavity is different from the beam that "fits" the
linear cavity.

For the spherical mirror, R, the effective radius of curvature in the horizontal axis is (23:42)

$$R_x = R \cos \theta \qquad \text{(A.3)}$$

where

$R_x$ = the effective radius of curvature of R in the horizontal axis

R = true radius of curvature

$\theta$ = angle of incidence to R

Similarly, the effective radius of curvature in the vertical axis is (23:42)

$$R_y = \frac{R}{\cos \theta} \qquad \text{(A.4)}$$

where

$R_y$ = effective radius of curvature of R in the vertical axis

The spherical mirror, R, acts as an elliptical mirror in the square cavity due to these astigmatic effects. The Gaussian beam that "fits" the square cavity is found independently in each of the axes. This generally causes the characteristic Gaussian beam of the cavity to have an elliptical spot.

Substituting the values for the radius of curvature of the cavity mirrors into Equations (A.3) and (A.4) and with the angle of incidence equal to 45 degrees, yields 565.68 cm and 1131.37 cm, respectively, for the horizontal
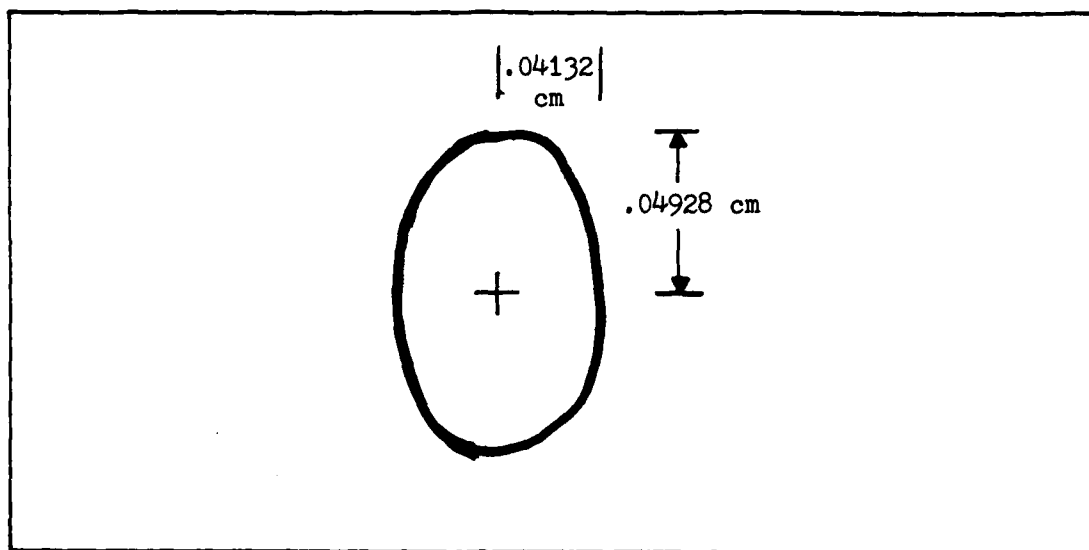
Fig. A.4. Cavity Spot Size at Beam Waist

and vertical effective radius of curvature. Using these values, Equation (A.2) is used to find the radius of the laser spot. The elliptical shape and dimensions are shown in Figure A.4. Once the characteristic modes of the laser and the cavity are determined, the entire beam of each can be characterized using Equations (2.22) and (2.23). By manipulation of Equation (2.22), the location along the beam where the cavity and laser spot sizes match (in the horizontal and vertical plane) can be found by solving the quadratic:

$$(\omega_{oL}^2 - \omega_{oC}^2) \; z^2 - 2x\omega_{oL}^2 \, z + x^2 \omega_{oL}^2$$

$$+ \; (\frac{\pi}{\lambda})^2 \; (\omega_{oL}\omega_{oC})^2 (\omega_{oC}^2 - \omega_{oL}^2) \; = \; 0 \qquad (A.5)$$

where

$\omega_{oL}$ = waist of the laser

$\omega_{oC}$ = waist of the cavity

x = distance between $\omega_{oC}$ and $\omega_{oL}$

z = distance from $\omega_{oL}$ where the spot sizes match

$\lambda$ = wavelength of the laser light

The radius of curvature of each beam at these points is then found using Equation (2.23). As shown in Figure A.5, the horizontal axis of the spots match at point A and the vertical axis of the spots match at point B. By inserting a cylindrical lens at the matching locations, A and B, it is possible to convert the radius of curvature of the cavity beam. The cylindrical lens has the property of only
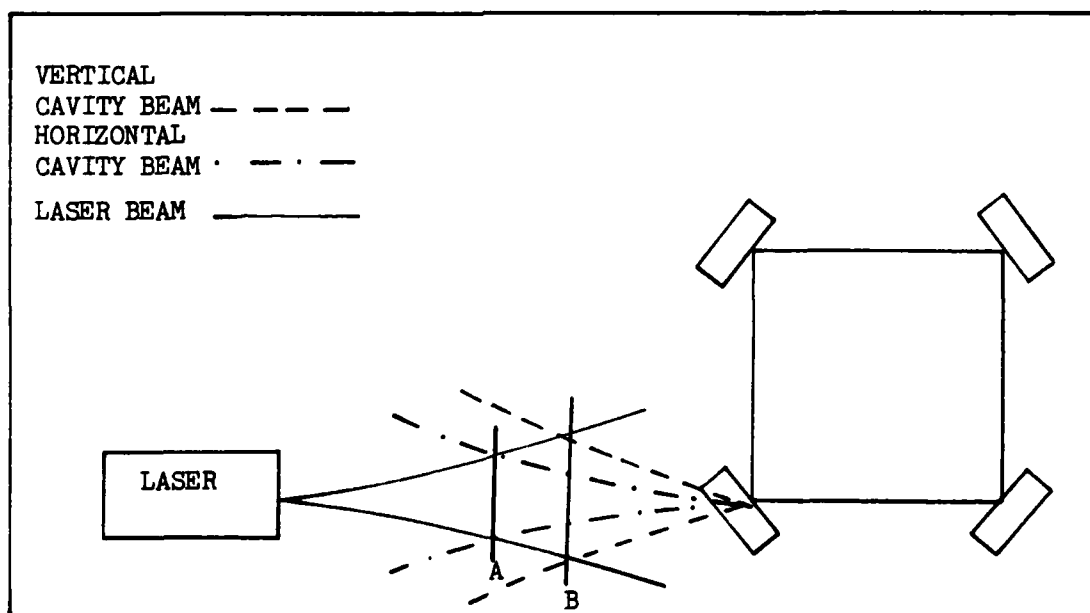
Fig. A.5. Mode Matching Using Two Cylindrical Lenses

82

focusing the beam in a single axis; the other axis of the beam is allowed to pass through unchanged. The focal length of the lens (F) must be (6):

$$F = \frac{R_C R_L}{R_C - R_L} \qquad (A.6)$$

where

$R_C$ = radius of curvature of cavity beam at lens

$R_L$ = radius of curvature of laser beam at lens

Applying the above procedure to the design gives the location and focal lengths of cylindrical lenses as shown in Table A.3.

TABLE A.3

MODE MATCHING LENS PLACEMENT

|  | Focal Length (mm) | Distance from Waist (cm) |
|---|---|---|
| Horizontal Axis | 700 | 61.27 |
| Vertical Axis | 842 | 64.17 |

One method to obtain an estimate of how well the laser is mode matched to the cavity is to determine the relative strengths of higher-order modes that will resonate in the cavity. Figure A.6 shows that several higher-order modes are present along with the $TEM_{0,0}$ mode when a 20 volt sinusoidal signal is applied to the PZTs of the

unmatched cavity (the dominant $TEM_{0,0}$ mode is represented by the large spike and the higher order modes are represented by the small spikes). Figure A.7 shows that, after mode matching, the amplitude of the spike corresponding to the $TEM_{0,0}$ mode has been increased while the amplitude of the spikes corresponding to the higher order modes has been reduced.



TRANSMITTED
INTENSITY
500 mV/div

SCAN
VOLTAGE
20 V/div
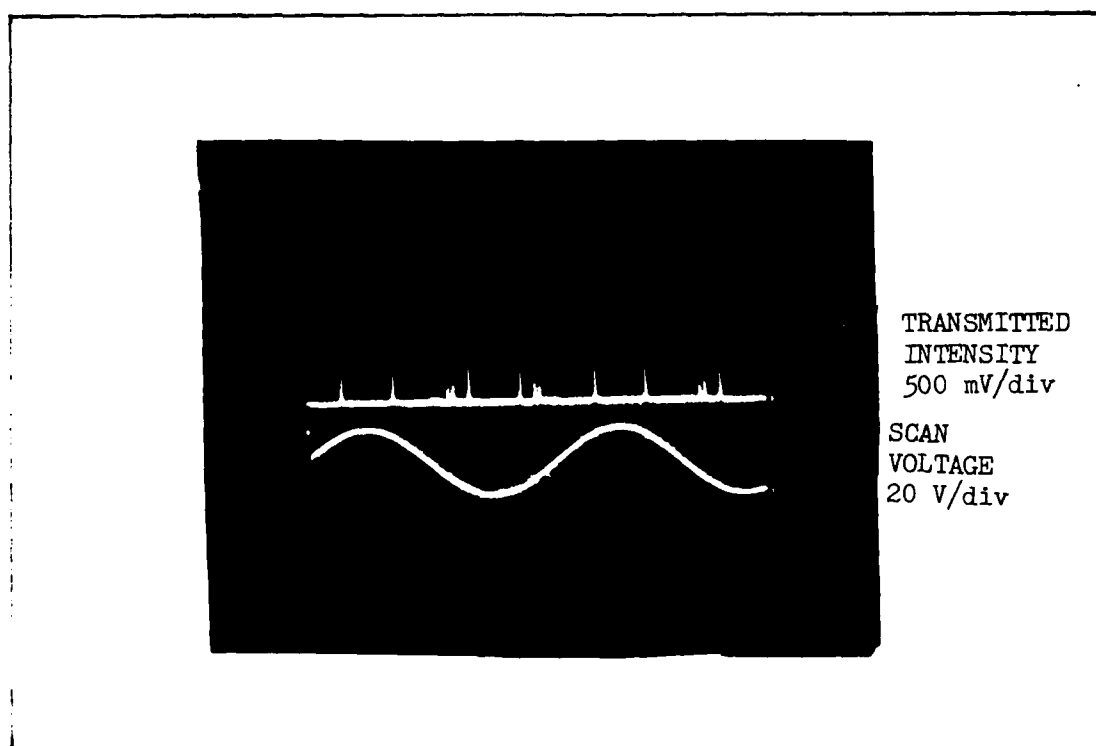
Fig. A.6.  Cavity Modes Present Before Mode Matching

TRANSMITTED INTENSITY
100 mV/div

SCAN VOLTAGE
1 V/div
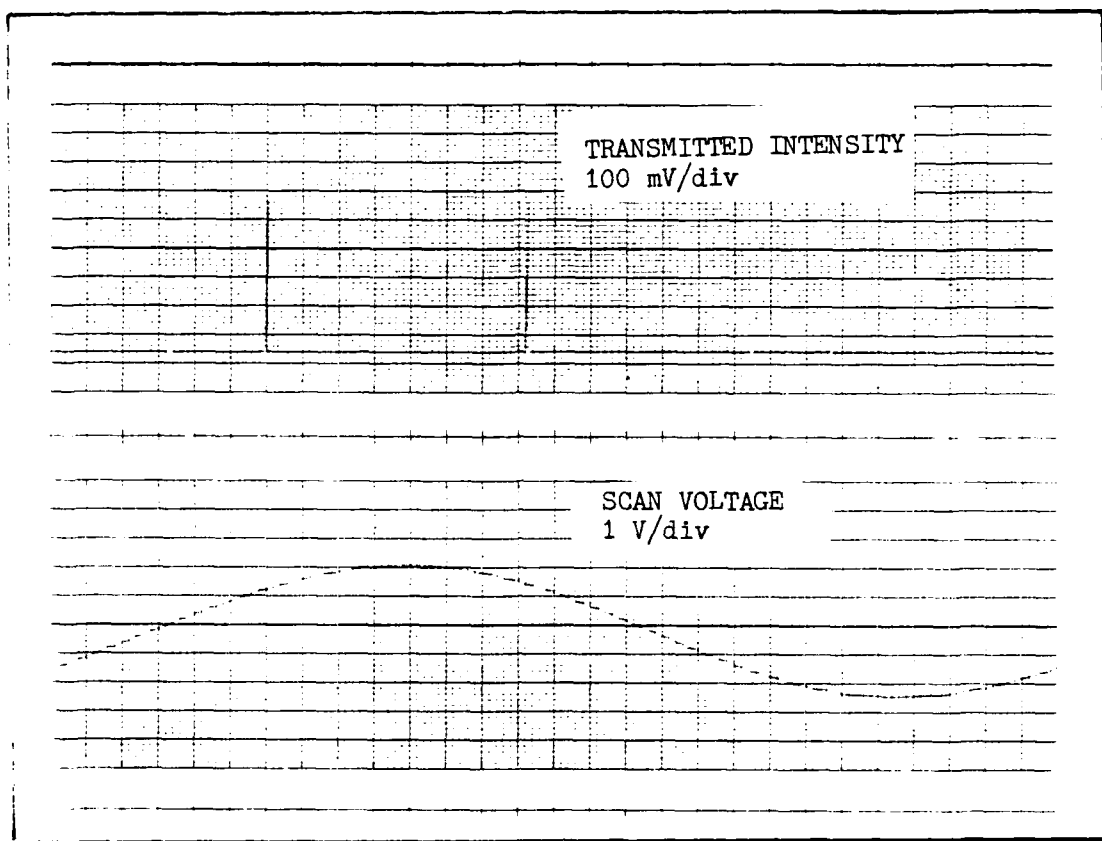
Fig. A.7.   Cavity Modes Present After Mode Matching
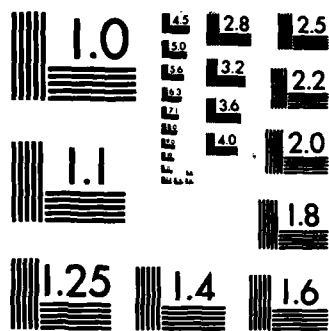
MICROCOPY RESOLUTION TEST CHART
ꓛARDS-1963-A

Appendix B: <u>Photodetector-Preamplifier</u> <u>Circuit</u>



United Detector Technology

UDT-455 HS Photodetector-Preamplifier
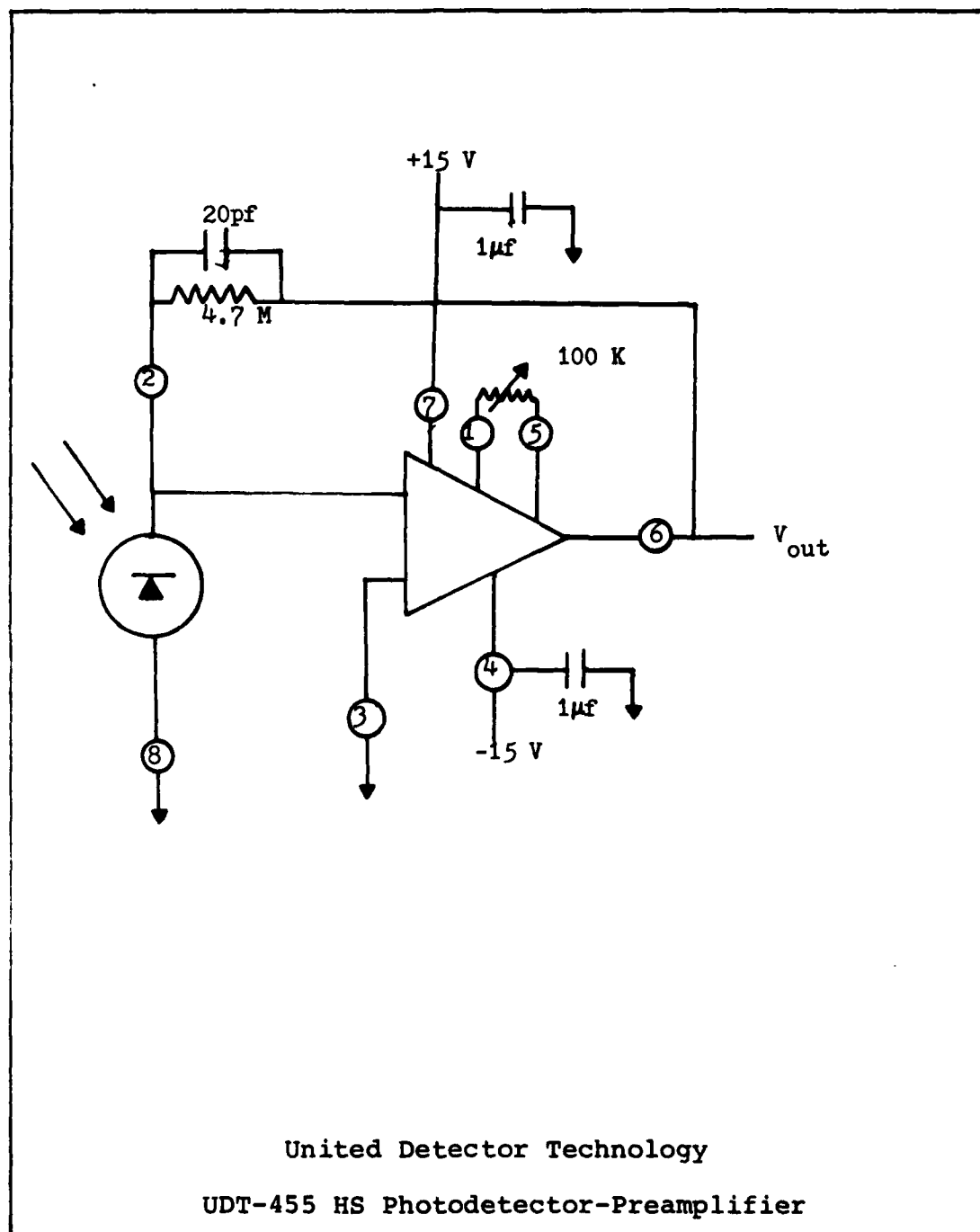
Fig. B.1.  Photodetector-Preamplifier Circuit

# Appendix C: Experimental and Data Reduction Procedures

## Test Set-up

Before measurements were taken, all equipment was allowed to warm up for at least 24 hours. This time was especially necessary, as the uncontrolled laser exhibits wide frequency variations after its initial turn-on. The large frequency change is beyond the controller capacity to lock on the resonant frequency of the cavity. Once the laser had stabilized (10-15 hours), the acquisition of frequency lock was possible.

To allow for data collection, a microcomputer was connected to the frequency counter and was programmed to sample the frequency difference information (corresponding to the rotation rate) at a 1 Hz rate. The reflected intensities from both beams, the intensity difference, and the LIA error signal were recorded on a strip chart recorder.

## Test Procedure

1. A 30 volt, 10 Hz signal was applied to the PZTs and the two reflected intensities were monitored on the oscilloscope. The steering mirrors and the translation stages were adjusted to maximize the $TEM_{0,0}$ mode of the cavity.

2.  For each LIA, the output was connected to the oscilloscope.  The 30 volt, 10 Hz scan signal was summed with the 3 millivolt, 30 KHz modulation signal (corresponding to one-half of the cavity linewidth) and applied to the PZTs.  The time constant of the LIA was set to MIN and the sensitivity was adjusted to allow for the maximum input signal from the detectors without overloading the LIA.  The error signal out of the LIA (discriminant) was maximized by adjusting the phase control on the LIA to give the minimum signal and then rotating the phase 90 degrees.  Figure C.1 shows the resulting discriminant along with the reflected intensity and the scan voltage.

3.  The LIA outputs were connected to the compensators.  The TUNE/LOCK switch on the laser controller was set to TUNE.  Table C.1 shows the switch positions and gain settings for both compensators (Figures 3.5 and 3.7) for lock acquisition.

4.  The bias voltage control on the PZT amplifier was adjusted to bring the cavity resonant frequency close to the laser frequency.  When the resonant mode was located, the reflected intensity dropped.  The 100 ohm resistor was taken out of the integrator circuit by opening a switch and the 27 K ohm resistor was added by closing a switch (See Figure 3.5).  Also the LOCK/TUNE switch on the laser controller was set to LOCK.  Usually both loops

88

REFLECTED
INTENSITY
500 mV/div

SCAN
VOLTAGE
10 V/div

DISCRIMINANT
500 mV/div
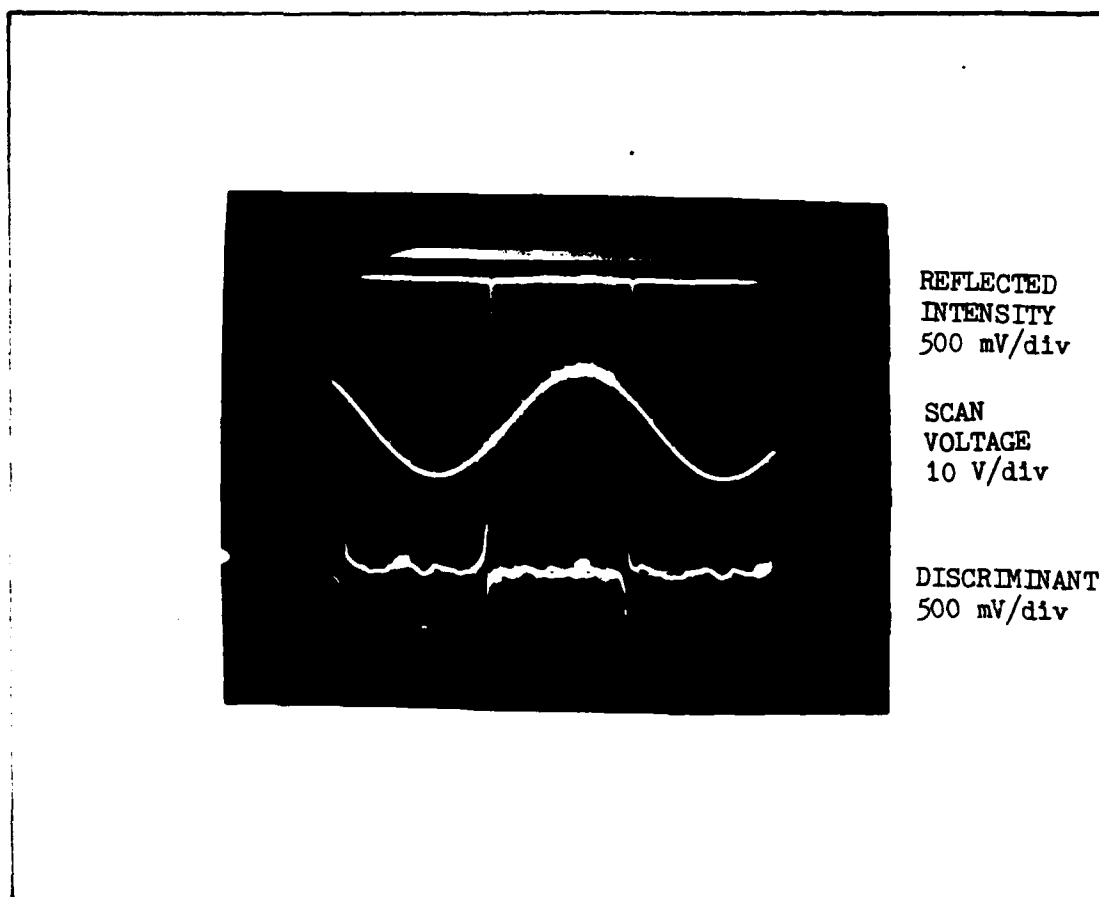
Fig. C.1.   Maximized Discriminant

## TABLE C.1

### COMPENSATOR SWITCH POSITIONS AND GAIN SETTINGS
### FOR LOCK ACQUISITION

|                  | Laser Loop | A/O Loop |
|------------------|:----------:|:--------:|
| Integrator       | ON         | ON       |
| 100 ohm          | ON         | ON       |
| 27 K ohm         | OFF        | OFF      |
| Summer           | N/A        | ON       |
| Lead             | 5.0        | 5.0      |
| Gain             | 5.0        | 5.0      |
| Integrator Null  | 5.0        | 5.0      |
| Bias             | 5.0        | *        |

*Adjusted so that the VCO output a 40 MHz signal.

locked to the resonant valley of the reflected intensity. If this did not occur, the step was repeated.

5.  Through observation of the signals on the analog recorder, the amplitude of the VCO signal was adjusted to minimize the intensity difference signal going into the secondary loop (LIA).

6.  The lead and gain potentiometers were adjusted to give the highest degree of lock as observed by connecting the FFT analyzer to the photodetector outputs. The adjustment which maximized the $2f_m$ frequency component (60 KHz) and minimized other components was chosen as the one that provided the best controller operation.

With these steps completed, the PRRLG was ready for testing.

## Data Reduction

The data recorded on the floppy disk corresponded to measurement of the difference frequency, $\Delta f$, between the two counterrotating beams. From Equation (2.39) the expected frequency was 11.6092 Hz. To determine bias, bias drift, and random error, a straight line was fit to the recorded data using a least-squares fit. The y-intercept of the fit line was compared to the expected 11.6092 Hz. The difference was defined as the bias. The slope of the line was defined to be the bias drift and the standard deviation of the residuals from the line was the random error.

## Appendix D: <u>Detailed Laser Stabilization</u> Observations

### <u>Cavity Lifetime</u>

To determine the effect cavity lifetime has on the closed loop laser frequency controller, consider Figure D.1. For this low loss, mode matched cavity at resonance, $I_c$ is very large, $I_t \sim I_o$, and $I_r \sim 0$. If losses are ignored then

$$I_t \sim I_c \times T_2$$

$$I_r \sim I_o(1-T_1) - I_c \times T_1$$

In order for $I \sim 0$, there must be a nearly perfect cancellation of the leakage field, $I_c \times T_2$, with the reflection of $I_o$, $[I_o \times (1-T_1)]$.

If the cavity is rotated, or if the physical path length is changed within the cavity, or if the phase of the incident light changes, there is an immediate loss of the nearly perfect cancellation in $I_r$. The effect of the phase change is not immediately seen in the transmitted intensity $I_t$ because of the large $I_c \times T_2$ component relative to the small $I_o \times T_1 \times T_2$ component. For the effect to be noticeable, the phase-shifted light must be stored up within the cavity so that the phase-shifted energy is

Laser diagram with labels:

LASER

$I_R$

$T_1$

$I_O$

$I_C$

$T_2$

$I_T$

$I_O$ - Incident Intensity
$I_R$ - Reflected Intensity
$I_T$ - Transmitted Intensity
$T_1$ - Mirror Transmission
$T_2$ - Mirror Transmission
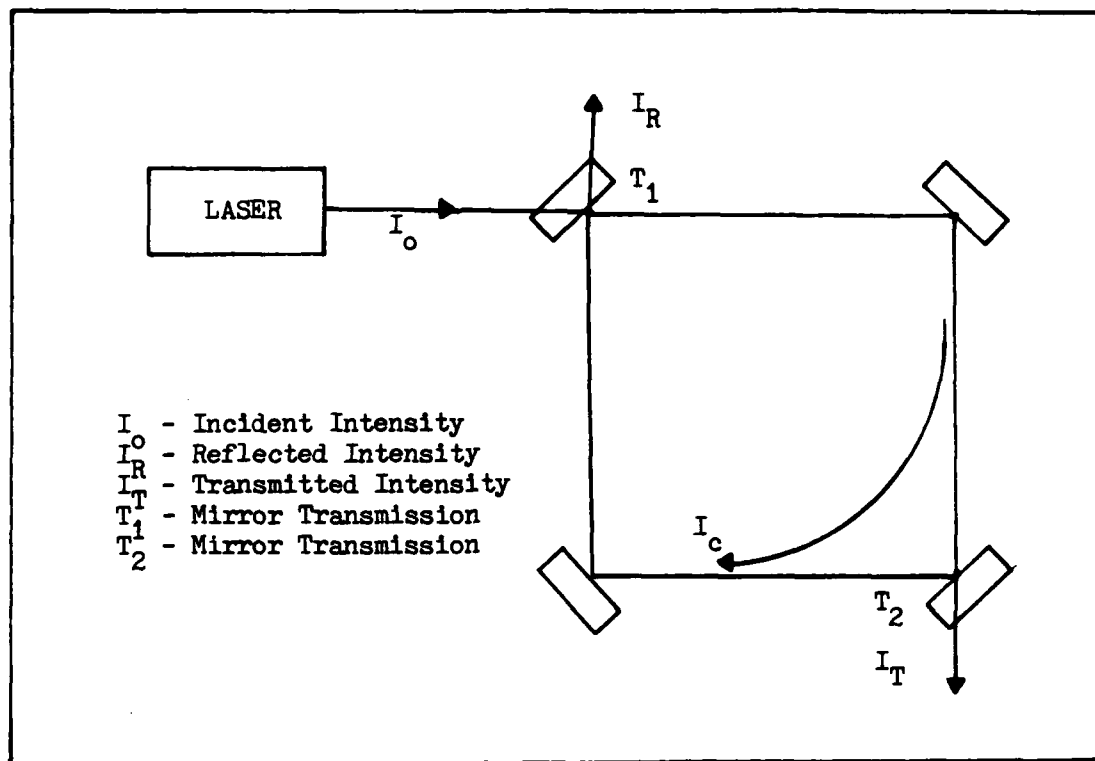
Fig. D.1.   Cavity at Resonance

now the dominant source of energy transmitted through the cavity.

In the above situation, there is a filtering effect of the incident light with a filter time constant on the order of the cavity lifetime.  This filtering effect prevents the observation of the rapid, random phase fluctuations in the incident light when the transmitted beam is monitored.  Hence, the concept of using the reflected beam to derive the error signal for the controller is considered.

This filtering effect is not a problem with the PRRLG used in this research because the cavity lifetime is

93

only about 14 microseconds, which is just outside the con-
troller bandwidth.  However, for the 58 $m^2$ PRRLG the
expected cavity lifetime is 1-2 milliseconds, which would
severely limit the bandwidth of the controller, probably
to the point that frequency lock to the cavity would not
occur.  Therefore, the use of the reflected beam for con-
trol purposes is recommended.

## Frequency Locking Laser to Cavity

As mentioned in Chapter III, the laser discharge
current control alone did not provide enough dynamic range
for the laser to remain locked to the cavity for long
periods of time.  Figure D.2 shows the results when using
only the current control to stabilize the laser frequency.
As shown, the intensity signal has several small spikes in
it which correspond to vibrations due to conversations,
and pressure changes due to the lab door being opened.
The error signal and the voltage going to the current con-
troller are correspondingly noisy at these points.  Also
both of these signals exhibit ramps, which indicate that
more and more control is needed to keep the beam in
resonance.  Finally after about 35 minutes, the controller
saturates, and lock is lost.

When the heater control is attached, many of the
observed problems clear up.  As seen in Figure D.3, the
intensity is no longer susceptible to the door being

94

opened or to minor vibrations. In addition, the noise on the error signal and control signals is greatly reduced. With the heater control added, lock can be maintained virtually indefinitely.

The noise frequency on the error signal was investigated by connecting the signal to a Fourier analyzer. This indicated a 60 Hz frequency components which what later traced to being injected into the system through the PZT modulation signal. When the modulation signal was set to maximize loop sensitivity, the signal to noise ratio was less than 3. In effect, the cavity resonant frequency was being perturbed at a 60 Hz rate. Since this was within the bandwidth of the controller, its effect was eliminated; however, the presence of the signal was still undesirable.

CURRENT CONTROL SIGNAL
500 mV/div

ERROR SIGNAL
1 V/div

REFLECTED INTENSITY
SIGNAL 20 mV/div

5 mm/min
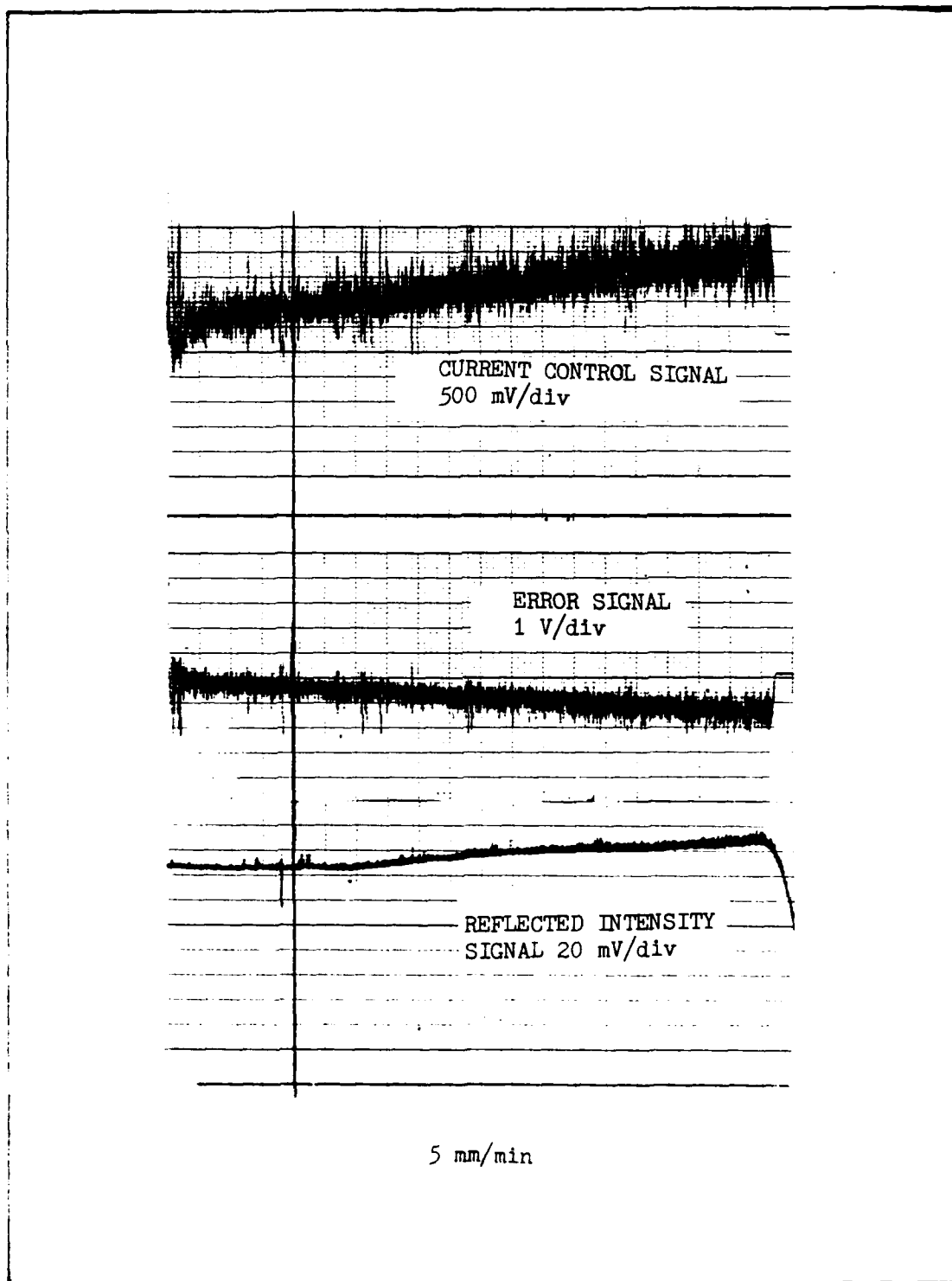
Fig. D.2.   Stabilization Using Current Control

96

HEATER VOLTAGE
50 mV/div

CURRENT CONTROL SIGNAL
500 mV/div

ERROR SIGNAL
1 V/div

REFLECTED INTENSITY
SIGNAL 20mV/div

5 mm/min
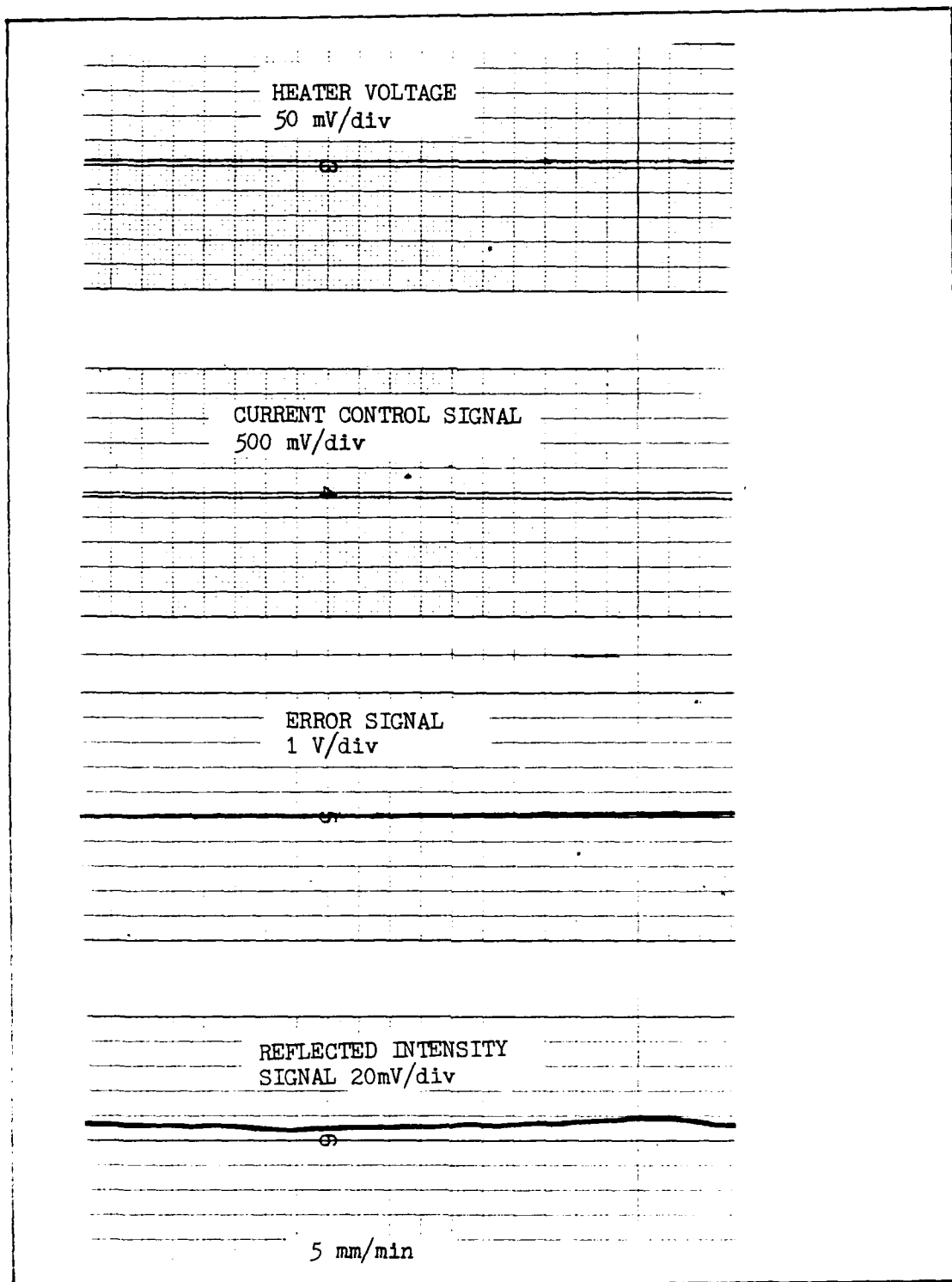
Fig. D.3. Stabilization Using Current and Heater Control

97

# Bibliography

1. Aronowitz, Frederick. "The Laser Gyro," _Laser Applications_, edited by Monte Ross. New York: Academic Press, 1971, pp. 134-200.

2. Drever, R. W. P., J. L. Hall, F. V. Kowalski, J. Hough, G. M. Ford, A. J. Munley, and H. Ward. "Laser Phase and Frequency Stabilization Using an Optical Resonator," _Applied Physics B_, _31_: 97-105 (1983).

3. Eckhardt, D. H. _Proceedings of the Society of Photo-Optics Instrumentation Engineers_, _157_: 172 (1978).

4. Ezekiel, S. "An Overview of Passive Optical Gyros," _Proceedings of the Society of Photo-Optics Instrumentation Engineers_, _487_: 13-17 (1984).

5. Ezekiel, S. and S. R. Balsamo. "Passive Ring Resonator Laser Gyroscope," _Applied Physics Letters_, _30_: 478-480 (1 May 1977).

6. Hall, J. L. Personal interviews. Joint Institute for Laboratory Astrophysics, Boulder CO, 15 Jun through 20 Sep 1985.

7. Hangan, M. P., M. O. Scully, and K. Just. "A Proposed Optical Test of Preferred Fame Cosmologies," _Physics Letters 77A_: 88 (1980).

8. Heer, C. V. "History of the Laser Gyro," _Proceedings of the Society of Photo-Optics Instrumentation Engineers_, _487_: 3 (1984).

9. Holland, Charles R. and David J. Olkowski. _Evaluation of Errors in a Passive Ring Laser Gyroscope_. MS thesis. Air Force Institute of Technology (AU), Wright-Patterson AFB OH, December 1978.

10. Ma, L. S., G. Kramer, and J. L. Hall. "Principles of Optical Phase Locking," (to be published in _Applied Physics B_).

11. Macek, W. M. and D. T. M. Davis, Jr. "Rotation Rate Sensing with Traveling-Wave Ring Lasers," _Applied Physics Letters_, _2_: 67-68 (February 1, 1963).

12. Nelson, Mark E. Implementation and Evaluation of Two Design Concepts of the Passive Ring Resonator Laser Gyroscope. MS thesis. Air Force Institute of Technology (AU), Wright-Patterson AFB OH, December 1983.

13. O'Shea, Donald C., W. Russell Callen and William T. Rhodes. Introduction to Lasers and Their Applications. Reading MA: Addison-Wesley Publishing Co., 1978.

14. Post, E. J. "Sagnac Effect," Reviews of Modern Physics, 39: 475-493 (April 1967).

15. Pugh, Keith A. Design, Construction, and Analysis of an Ultra-Low Expansion Quartz Resonant Cavity Passive Ring Resonator Laser Gyroscope. MS thesis. Air Force Institute of Technology (AU), Wright-Patterson AFB OH, December 1982.

16. Rosenthal, A. H. "Regenerative Circulatory Multiple-Beam Interferometry for the Study of Light-Propagation Effects," Journal of the Optical Society of America, 52: 1143-1148 (October 1962).

17. Sagnac, G. Computes Rendus Acadamie Des Sciences (Paris), 157: 708 (1913).

18. Sanders, G. A., M. G. Prentiss, and S. Ezeliel. "Passive Ring Resonator Method for Inertial Rotation Measurement in Geophysics and Relativity," Optics Letters, 6: 569-571 (November 1981).

19. Savage, P. G. "Strapdown Inertial Navigation Lecture Notes." Minnetonka MN: Strapdown Associates, Inc., 1981.

20. Shaw, G. L. and B. J. Simmons. "A 58 $m^2$ Passive Resonant Ring Laser Gyroscope," Proceedings of the Society of Photo-Optics Instrumentation Engineers, 478: 117 (May 1984).

21. Siegman, A. E. An Introduction to Lasers and Masers. New York: McGraw-Hill Book Company, 1971.

22. Tehrani, M. M. and J. A. Hoschette. "The Passive Cavity Gyro," Proceedings of the Society of Photo-Optics Instrumentation Engineers, 412: 234-239 (1984).

23. Verdeyen, Joseph T. Laser Electronics. Englewood Cliffs NJ: Prentice-Hall, Inc., 1981.

24. Wilson, J. and J. F. B. Hawkes. Optoelectronics: An Introduction. Englewood Cliffs NJ: Prentice-Hall, Inc., 1983.

25. Yariv, Amnon. Introduction to Optical Electronics. New York: Holt, Rinehart and Winston, Inc., 1971.

26. Zarinetchi, F., R. E. Meyer, G. A. Sanders, and S. Ezekiel. "Passive Resonator Gyro," Proceedings of the Society of Photo-Optics Instrumentation Engineers, 478: 122-127 (1984).

## VITA

Capt Mark A. Lorenz was born in Columbus, Ohio on 6 August 1959. He graduated from Agua Fria Union High School in Avondale, Arizona in 1977 whereupon he accepted an appointment to the USAF Academy. He graduated from the Academy with a Bachelor of Science in Engineering Sciences in 1981. Upon graduation, he was commissioned in the USAF and assigned to the 6585th Test Group at Holloman AFB. At this assignment he served as an inertial component and inertial navigation systems analyst. He entered the Air Force Institute of Technology in 1984 to work towards a Masters Degree in Guidance and Control. After graduating in December 1985, he was assigned to the Department of Astronautics at the USAF Academy.

Permanent address:   417 Sagebrush

Litchfield Park, AZ   85340

*A D-A114 309*

# REPORT DOCUMENTATION PAGE

| 1a. REPORT SECURITY CLASSIFICATION | 1b. RESTRICTIVE MARKINGS |
|---|---|
| UNCLASSIFIED | |

| 2a. SECURITY CLASSIFICATION AUTHORITY | 3. DISTRIBUTION/AVAILABILITY OF REPORT |
|---|---|
| | Approved for public release; |
| 2b. DECLASSIFICATION/DOWNGRADING SCHEDULE | distribution unlimited |

| 4. PERFORMING ORGANIZATION REPORT NUMBER(S) | 5. MONITORING ORGANIZATION REPORT NUMBER(S) |
|---|---|
| AFIT/GE/ENG/85D-24 | |

| 6a. NAME OF PERFORMING ORGANIZATION | 6b. OFFICE SYMBOL (If applicable) | 7a. NAME OF MONITORING ORGANIZATION |
|---|---|---|
| School of Engineering | AFIT/ENG | |

| 6c. ADDRESS (City, State and ZIP Code) | 7b. ADDRESS (City, State and ZIP Code) |
|---|---|
| Air Force Institute of Technology Wright-Patterson AFB, Ohio 45433 | |

| 8a. NAME OF FUNDING/SPONSORING ORGANIZATION | 8b. OFFICE SYMBOL (If applicable) | 9. PROCUREMENT INSTRUMENT IDENTIFICATION NUMBER |
|---|---|---|
| Frank J Seiler Research Laboratory | FJSRL/NH | |

| 8c. ADDRESS (City, State and ZIP Code) | 10. SOURCE OF FUNDING NOS. | | | |
|---|---|---|---|---|
| USAF Academy CO 80840 | PROGRAM ELEMENT NO. | PROJECT NO. | TASK NO. | WORK UNIT NO. |
| | | | | |

**11. TITLE** *(Include Security Classification)*
See Box 19

**12. PERSONAL AUTHOR(S)**
Mark A. Lorenz, B.S., Captain, USAF

| 13a. TYPE OF REPORT | 13b. TIME COVERED | 14. DATE OF REPORT (Yr., Mo., Day) | 15. PAGE COUNT |
|---|---|---|---|
| MS Thesis | FROM _____ TO _____ | 1985 December | 113 |

**16. SUPPLEMENTARY NOTATION**

| 17. COSATI CODES | | | 18. SUBJECT TERMS *(Continue on reverse if necessary and identify by block number)* |
|---|---|---|---|
| FIELD | GROUP | SUB. GR. | Passive Ring Laser Gyroscope, Laser Frequency Stabilization, High Finesse Resonant Cavity |
| 17 | 07 | | |
| 20 | 05 | | |

**19. ABSTRACT** *(Continue on reverse if necessary and identify by block number)*

Title:  A LASER FEEDBACK CONTROL DESIGN FOR PASSIVE RING LASER GYROS IN A VERY HIGH FINESSE CAVITY

Thesis Chairman:  Daniel J. Biezad, Lt Col, USAF
Deputy Head
Department of Electrical Engineering

Approved for public release: IAW AFR 190-1/.
LYNN E. WOLAVER 16 JAN 86
Dean for Research and Professional Development
Air Force Institute of Technology (ATC)
Wright-Patterson AFB OH 45433

| 20. DISTRIBUTION/AVAILABILITY OF ABSTRACT | 21. ABSTRACT SECURITY CLASSIFICATION |
|---|---|
| UNCLASSIFIED/UNLIMITED ☒ SAME AS RPT. ☐ DTIC USERS ☐ | UNCLASSIFIED |

| 22a. NAME OF RESPONSIBLE INDIVIDUAL | 22b. TELEPHONE NUMBER (Include Area Code) | 22c. OFFICE SYMBOL |
|---|---|---|
| Daniel J. Biezad, Lt Col, USAF | 513-255-3576 | AFIT/ENG |

**DD FORM 1473, 83 APR**  EDITION OF 1 JAN 73 IS OBSOLETE.

The Frank J. Seiler Research Laboratory is currently developing a Passive Resonant Ring Laser Gyroscope (PRRLG) enclosing 58 m$^2$ for proposed use in testing high precision rate sensors and for possibly validating the Theory of General Relativity. The sensitivities required for such experiments are in the $10^{-7}$ to $10^{-10}$ Earth Rate Unit (ERU) range. This high sensitivity necessitates the use of a large, high finesse cavity.

In dealing with high finesse cavities new considerations arise. For example, the cavity linewidth is narrower than linewidths of commercially available stabilized He-Ne lasers. The stability of the laser then becomes the limiting factor in the performance of the PRRLG because of the increased signal-to-noise ratio that arises in this situation. In addition, high finesse cavities exhibit photon lifetimes on the order of $10^{-3}$ to $10^{-6}$ seconds, which limits the bandwidth of practical controllers.

In this research, a PRRLG was constructed in which a He-Ne laser was frequency locked to 25,000 finesse, 169 cm$^2$ resonant cavity, as opposed to the more traditional technique of locking the resonant condition of the cavity to the laser frequency. Using this configuration a random error of 0.0078 ERU for an averaging time of 10 seconds was observed. The major error sources found in the gyro were identified and methods to eliminate them were proposed. Extrapolation of the performance of this PRRLG to the much larger 58 m$^2$ PRRLG, indicates the desired sensitivity for precision testing and relativity experiments is achievable.

# END

FILMED

3

-86

DTIC